

Florian Hofer

# Computational Properties of L5 Pyramidal Cells

Master Thesis

Graz University of Technology

Institute for Theoretical Computer Science

Head: o.Univ.-Prof. Dr. Wolfgang Maass

Supervisor: o.Univ.-Prof. Dr. Wolfgang Maass

Graz, July 2014

## Statutory Declaration

I declare that I have authored this thesis independently, that I have not used other than the declared sources/resources, and that I have explicitly marked all material which has been quoted either literally or by content from the used sources.

Graz, \_\_\_\_\_  
Date Signature

## Eidesstattliche Erklärung<sup>1</sup>

Ich erkläre an Eides statt, dass ich die vorliegende Arbeit selbstständig verfasst, andere als die angegebenen Quellen/Hilfsmittel nicht benutzt, und die den benutzten Quellen wörtlich und inhaltlich entnommenen Stellen als solche kenntlich gemacht habe.

Graz, am \_\_\_\_\_  
Datum Unterschrift

---

<sup>1</sup>Beschluss der Curricula-Kommission für Bachelor-, Master- und Diplomstudien vom 10.11.2008; Genehmigung des Senates am 1.12.2008

# Abstract

In this master thesis recent findings about the function and behaviour of layer 5 pyramidal neurons are outlined. The main focus lies on a secondary spiking mechanism, the calcium spike, and how it is able to boost the computational properties of single pyramidal neurons.

The practical part will deal with the design and implementation of a simple layer 5 pyramidal neuron with additional compartments modelling two dendritic areas separately. These areas are able to influence each other via active signal propagation. Further an internal calcium spiking mechanism is added, which triggers an output burst.

The model behaviour is further compared with experimental results and showed to reproduce the results obtained by [Larkum, 2013]. Some additional simulations are carried out, which show how hidden parameters can be automatically obtained from the model behaviour and how the bursting mechanism can be used for learning.

# Kurzfassung

In dieser Masterarbeit werden die neuesten Entwicklungen und Erkenntnisse über die Funktion und das Verhalten von Layer 5 Pyramidenneuronen vorgestellt. Der Hauptfokus liegt hierbei bei dem sekundären Spiking Mechanismus, dem Kalzium Spike, und dessen Auswirkungen auf die Rechenleistung und Komplexität von einzelnen Pyramidenneuronen.

Der praktische Teil der Arbeit beschäftigt sich mit dem Design und der Implementierung von einfachen Layer 5 Pyramidenneuronen mit zusätzlichen Compartments, welche zwei dendritische Regionen getrennt modellieren. Diese Compartments sind in der Lage, sich gegenseitig über aktive Signalpropagierung zu beeinflussen. Außerdem verfügt das Modell über einen internen Kalzium Spike Mechanismus, welcher einen Burst an Spikes am Ausgang auslösen kann.

Das Modell wird zuletzt mit experimentellen Resultaten verglichen und es zeigte sich dass die Resultate von [Larkum, 2013] reproduziert werden konnten. Zusätzlich werden Simulationen angeführt, die zeigen wie versteckte Parameter des Modells automatisch extrahiert werden können und wie der Bursting Mechanismus für das Lernen von synaptischen Gewichten verwendet werden kann.

# Table of Contents

<b>Abstract</b>	<b>iii</b>
<b>Kurzfassung</b>	<b>iv</b>
<b>1 Introduction</b>	<b>1</b>
1.1 About Pyramidal Neurons . . . . .	1
1.2 Current Modelling Problems . . . . .	4
<b>2 State of the Art</b>	<b>5</b>
2.1 Modelling Principles . . . . .	5
2.2 Neural Network Representations . . . . .	6
2.3 Compartmental Models . . . . .	8
<b>3 Theory</b>	<b>10</b>
3.1 Pyramidal Neuron Properties . . . . .	10
3.1.1 Calcium Spikes . . . . .	13
3.1.2 NMDA Spikes . . . . .	15
3.1.3 Use of Dendrites . . . . .	16
3.1.4 Coincidence Detection . . . . .	18
3.1.5 Inhibition & Coupling . . . . .	20
3.1.6 Plasticity . . . . .	23
3.2 Neuron Modelling . . . . .	25
3.2.1 Spike Response Model . . . . .	25
3.2.2 Stochasticity . . . . .	26
3.3 NEST Simulation Environment . . . . .	27
<b>4 Concept</b>	<b>30</b>
4.1 Pyramidal Neuron Model . . . . .	30
4.1.1 Requirements . . . . .	30

## Table of Contents

4.1.2	Simplifications . . . . .	31
4.1.3	Model Schematic . . . . .	32
4.1.4	Model Description . . . . .	34
4.2	Simulation Concept . . . . .	42
4.2.1	Simulation Objectives . . . . .	42
4.2.2	Parameter Learning Algorithm . . . . .	43
<b>5</b>	<b>Implementation</b>	<b>53</b>
5.1	General description . . . . .	53
5.2	Mathematical translation . . . . .	54
5.2.1	EPSP Kernel . . . . .	54
5.3	NEST Simulation Parameters . . . . .	58
5.3.1	General Parameters . . . . .	58
5.3.2	Apical Compartment . . . . .	59
5.3.3	Oblique Compartment . . . . .	60
5.3.4	Somatic Compartment . . . . .	61
5.3.5	Basal Compartment . . . . .	62
5.4	Simulation Results . . . . .	63
5.4.1	Comparison to Larkum Paper . . . . .	63
5.4.2	Comparison to Naud Paper . . . . .	69
5.4.3	Coincidence Detection via Manual Parameter Tuning . . . . .	73
5.4.4	Learning Algorithm . . . . .	77
<b>6</b>	<b>Conclusion</b>	<b>86</b>
6.1	Results . . . . .	86
6.2	Outlook . . . . .	87
	<b>References</b>	<b>89</b>

# List of Figures

1.1	Typical L5 pyramidal neuron . . . . .	2
2.1	Neuron model representation as a two-layer neural network . . . . .	7
3.1	Spike initiation zones in pyramidal neurons . . . . .	12
3.2	Concept of three possible ways to combine two information streams in neurons . . . . .	20
4.1	Conceptual l5 pyramidal neuron model . . . . .	33
4.2	HMM Simulation model . . . . .	44
4.3	Discretized somatic membrane potential . . . . .	49
4.4	State transition matrix A . . . . .	50
4.5	Spike probability matrix B . . . . .	51
5.1	Alpha synapse function and membrane potential . . . . .	57
5.2	BAC mechanism from Larkum et al. . . . .	64
5.3	Simulation of an apical input spike . . . . .	65
5.4	Simulation of a basal input current . . . . .	66
5.5	Simulation of a combined apical spike/basal current input . . . . .	67
5.6	Current comparison during spikes and bursts by Naud et al. . . . .	70
5.7	Average current around spikes and bursts . . . . .	71
5.8	Neural Network, possible connection model . . . . .	74
5.9	Possible neuron activity, Layer one . . . . .	75
5.10	Possible neuron activity, Layer two . . . . .	76
5.11	Pyramidal Neuron Simulation with adaptive weights, start schematic . . . . .	78
5.12	Pyramidal Neuron Simulation with adaptive weights, end schematic . . . . .	79
5.13	Pyramidal Neuron Simulation with adaptive weights, start result apical . . . . .	82

## List of Figures

5.14	Pyramidal Neuron Simulation with adaptive weights, end result apical . . . . .	83
5.15	Pyramidal Neuron Simulation with adaptive weights, start result basal . . . . .	84
5.16	Pyramidal Neuron Simulation with adaptive weights, end result basal . . . . .	85

# 1 Introduction

## 1.1 About Pyramidal Neurons

Pyramidal neurons, named after the pyramidal shape of their soma, are found in the cerebral cortex, the hippocampus and the amygdala of all mammals studied so far [Scholarpedia, 2013b]. Layer 5 (L5) pyramidal neurons have an apical as well as a basal dendritic tree, where the apical dendrites extend up to layer 1 [Murayama and Larkum, 2009] [Larkum et al., 2001]. This dendritic structure allows pyramids to receive a complex set of inputs from all cortical layers. The axon of a pyramidal cell can even extend further reaching both intra-cortical and subcortical areas [Manns et al., 2004]. A typical sketch of a L5 pyramidal cell with outlined cortical layers on the left can be seen in figure 1.1.

## 1 Introduction

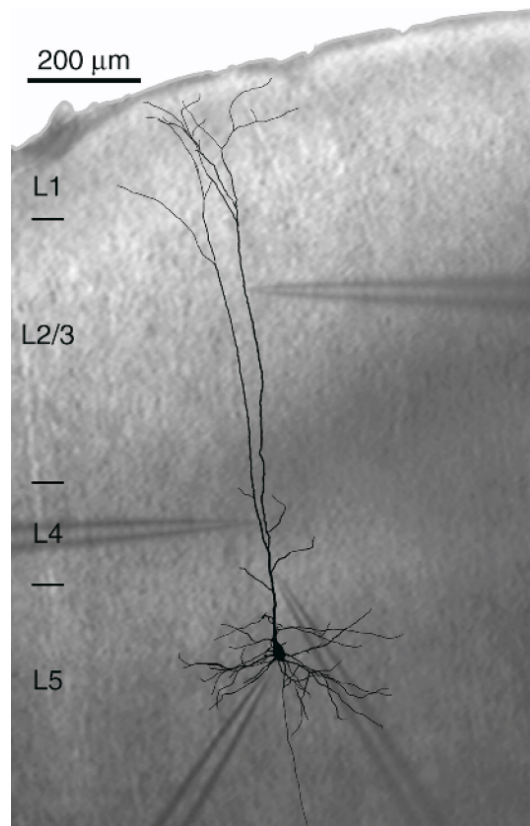


Figure 1.1: Typical L5 pyramidal neuron, taken from [Larkum et al., 2001]. The assigned layers are plotted on the left. The drawing shows the cell body in layer 5 with the apical dendritic tree going up to layer 1.

As 70% to 80% of the cortex consists of pyramids, they are proposed to be the main determining factor for the superior performance of the cortex in comparison to other brain regions [Larkum, 2013].

To date the cortex is believed to contribute to effects such as perceptual learning and memory [Squire, 2004], and even consciousness [Crick and Koch, 1998] [Merker, 2007]. Although Merker lined out the Sprague effect, which could prove that the neocortex simply acts as a medium for higher perceptual functions such as attention and consciousness and that the evolutionary older regions of the brain, namely the midbrain and brainstem

## 1 Introduction

areas are the main functional core which just uses the cerebral cortex as a storage and calculation unit. Nevertheless they acknowledge that the cortex is still an essential unit for consciousness.

As Larkum et al. [Larkum, 2013] already lined out, pyramidal neurons are the most ubiquitous neuron type in the cortex. Elston [Elston, 2003] further investigates the role of different pyramidal neuron structure on functional segregation in cortical areas. The paper shows evidence that the complexity of pyramidal neurons, including the size of their axonal and dendritic connections, their branching pattern and the number and distribution of synaptic inputs, varies across different functional areas, such as the pre-frontal cortex and the visual processing areas V1 and V2. It is therefore suggested that, although all cortical areas consist mostly of pyramids, the specialized structure of the cells determines function.

This view can be combined with an in vitro experiment on mice carried out to project slightly different L5 pyramidal neuron morphology to their axonal target region. The experiment showed that pyramids connecting to outer-cortical regions show varying features including dendritic branch counts and the width of dendritic tufts depending on their projection area [Hattox and Nelson, 2007].

The importance of an exact modelling of pyramidal neuron structures was also demonstrated for memory tasks. Poirazi et al. showed that memory could be explained not only by means of synaptic plasticity, but also by the addressing of synaptic inputs on the dendritic tree. Various experiments in vitro and in vivo mentioned in the paper have shown that axonal and dendritic structures are able to change and emerge within minutes. Moreover, the advantages of a compartmental model are lined out, as multiple separate integration units in the dendrites are able to account for a much higher memory capacity compared to single summation units [Poirazi and Mel, 2001].

### 1.2 Current Modelling Problems

The current problems in modelling the behaviour of pyramidal neurons can be attributed to a large extent on the little understanding of their physiology. Many papers have already raised the necessity of differentiating at least between complex pyramidal cells, which are most common (up to 89%) in the prefrontal cortex and simple pyramidal cells, which are common in the primary visual cortex [Wang et al., 2006]. As is reviewed in section 3.1.6, not only the plasticity, but the whole transfer function and behaviour (depression or facilitation) of synapses between interneurons and pyramids and in between pyramids can change within minutes. Combined with the fact that pyramidal neurons have 10.000-100.000 excitatory synapses and 1.000-10.000 inhibitory synapses [Spruston, 2008] [Scholarpedia, 2013b], but also see Destexhe et al. [Destexhe and Pare, 1999] who defines 5.000-60.000 synaptic connections, this leads to a great modelling issue which is not concerned.

In addition to the exact definition of synaptic connections, the distribution of voltage-gated ion channels has to be taken into consideration. It has been proven that these channels are the main generating power behind dendritic spikes. However, there is still no general rule determining the distribution of these channels in pyramidal neuron dendrites [Häusser et al., 2000]. It could only be proven that their distribution changes during the brain development and that they can be influenced and modulated by neurotransmitters.

Apart from the obvious missing features Körding and König explained that simplifications of neuron models are necessary, as the simulation of large networks with full-detailed neuron models are impossible with modern computational resources [Körding and König, 2001]. Nevertheless they argue that minor changes in neuronal models, like stepping away from the standard point neuron model and including a secondary integration area in dendrites, can still be simulated in large networks. A second integration site would increase the computational power of neurons, allowing a larger class of neural network algorithms to be implemented (see section 3.1.1).

## 2 State of the Art

The practical part of this thesis deals with the implementation of a layer 5 pyramidal neuron model with active dendrites. This chapter provides information about similar models, which have already been implemented. The first section (2.1) will list some general suggestions which have been made concerning the structure of pyramidal neuron models. The theoretical and experimental findings leading to these suggestions are described in chapter 3.

The subsequent sections will deal with the two most favoured concepts of pyramidal neuron modelling: The representation as a two-layer neural network (section 2.2) and as a compartmental model (section 2.3).

### 2.1 Modelling Principles

A recent review paper ([Major et al., 2013], especially figure 4) provides an overview of some of the current modelling principles of pyramidal neurons. Häusser et al. state that, in respect to a dendritic spiking mechanism, it was observed that action potentials (APs) from the soma do not fully propagate into the distal dendritic tree. As dendritic spikes still occur without the backpropagating AP triggering it, it was therefore proposed that at least a two-compartmental model is needed to account for the different spiking behaviour. Two compartments, a proximal compartment consisting of the soma, basal dendrites and axon triggering  $Na^+$  (sodium) spikes and a distal compartment modelling the apical dendrites where fast  $Na^+$  and slow  $Ca^{2+}$  (calcium) spikes are initiated.

The paper further states that the coupling between these two zones depends

## 2 State of the Art

on the oblique dendrites in between (see section 3.1.5). They therefore propose a 3-compartment model including a coupling zone [Häusser and Mel, 2003].

Major et al. on the other hand object that the formalization of the neuron in three compartments ignores the possibility of local computations performed in thin basal, oblique and tuft dendrites. These computations may be caused by small sodium spikes or NMDA spikes (see section 3.1.2). They further state that these effects are partially captured by a 2 or 3-layer feedforward neural network. However, this formalization would counteract with the former proposal of backpropagating APs, as no backpropagation can be modelled in a feedforward network [Major et al., 2013].

### 2.2 Neural Network Representations

The first paper mentioned here tries to model two sites of synaptic integration including a second spike initiation zone (dendritic calcium spikes) with the use of a two-layer neural network.

Based on the experimental results that postsynaptic bursting leads to LTP [Pike et al., 1999] and that a dendritic calcium spike is able to trigger bursting behaviour (see section 3.1.1) they proposed that the calcium spike is mostly used for learning. To test their prediction a two-layer neural network is used, with one input layer defined as a 4x4 or 9x9 raster which defines the first input stream for the output neuron. The second stream consists of an inhibitory signal of all other output neurons and is used as a learning signal.

An additional learning signal is added to the input stream concerning learning as supervised learning is used. Biologically the second input stream can be considered as a mixture of the backpropagating potential from the soma in pyramidal neurons with apical dendritic input while the first layer of the network can be considered as the input stream for proximal dendrites.

The paper neglects the influence of forward propagating potentials from apical dendrites to the soma. They justify this simplification, as a forward propagating voltages would influence the firing rate of the neuron and

## 2 State of the Art

therefore interfere with the output. In this case no separation between a preferred input-output function and the abstract learning signal can be made [Körding and König, 2000].

In another approach an error-backpropagating network is used to describe the two main dendritic trees of pyramidal neurons. Each of the two dendrites is receiving two input streams, which are summed up linearly and forwarded to the second layer of the network, representing the soma. The authors favour an artificial neural network representation over a compartmental model as the exact biophysical foundations for a compartmental representation of the dendrites is unknown. The neural network is used to teach both dendrites an individual input-output transfer function [Ryder and Favorov, 2001]. The following figure 2.1 shows a representation of the proposed model.

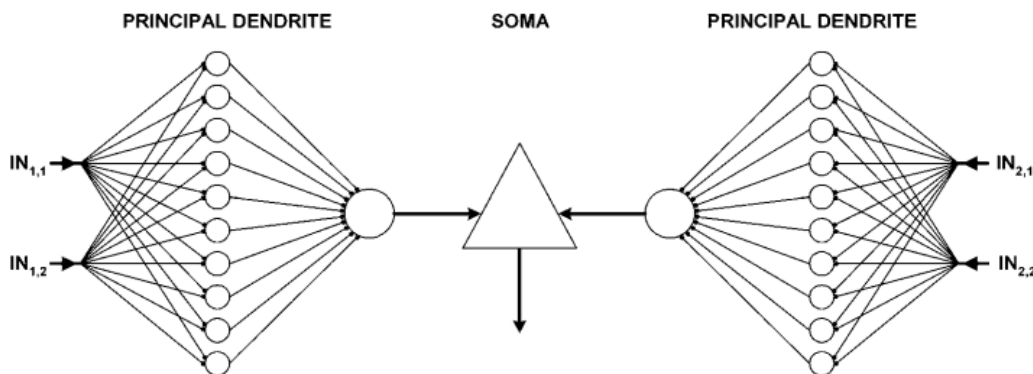


Figure 2.1: Neuron model representation as a two-layer neural network, figure taken from [Ryder and Favorov, 2001]. The two modelled dendrites are shown on the left and right side of the soma (triangle in the middle). Each dendrite receives two input streams, which serve as the first layer of the network. The input streams are afterwards summed up and forwarded to the soma in the center, representing the second layer of the neural network.

The last neural network representation mentioned here is not based on cortical layer 5 pyramids, but on hippocampal CA1 pyramidal neurons.

## 2 State of the Art

However, this study provides a good example of the mapping of active dendrites onto an abstract two-layer neural network.

The dendritic tree was therefore separated in several areas based on its spatial distribution. Each of these areas is treated as a separate thresholded subunit providing the first layer of the neural network. The output of these units is afterwards summed and again thresholded to get the whole cell response. The simulation proved that it produced the same output firing rate as a compared multi-compartment model with 21 different types of ion channels [Poirazi et al., 2003].

Based on the theoretical chapter in this thesis the representation of this model could also be compared to spatially distributed NMDA spikes (see section 3.1.2).

### 2.3 Compartmental Models

This section will focus on compartmental models of cortical pyramidal neurons. Only simple models (consisting of two to three compartments) will be taken into consideration.

[Larkum et al., 2004] models a two compartmental integrate-and-fire (IAF) model described by differential equations. A somatic and a dendritic compartment was used. The objective was to show that the active properties of dendrites are used to backpropagate the somatic action potential and perform a gain modulation along the dendritic path. This modulation increases the influence of distal synaptic inputs, which contribute to the overall neuron response in return (see section 3.1.4 for a better explanation). The simulation results could be matched to experimental data.

Jadi et al. also used a two-compartmental model, mapping a somatic and a dendritic compartment described by differential equations. The two compartments were connected, allowing a dendritic current to passively spread to the somatic compartment. The model was used to show the different effects of inhibitory synaptic input depending on the location (either targeted at the somatic or the dendritic compartment). They showed that

## 2 State of the Art

the two-compartmental model could reproduce the effects compared to a complex compartmental model consisting of 268 biophysically detailed compartments as well as experimental findings in vitro [Jadi et al., 2012].

[Ilan et al., 2011] also used a two-compartment model of a layer 5 pyramid, this time to demonstrate the effects of calcium spikes on the output function of the neuron. The model was described using ion channel densities, short time plasticity was performed using STDP. The simulation especially focused on the coupling effects in between the somatic and dendritic compartment. With correct parameter tuning the results could be matched to experimental data, showing that the coupling between the compartments varies over time.

Siegel et al. focused on the simulation of a conductance-based neuron model, described by a mixture of leaky integrate-and-fire equations and ion-channel summations. The neuron was split into two main areas, one receiving proclaimed top-down input and the other bottom-up (or sensory) input. Their mathematical formalization allowed the active propagation of potentials between the compartments. Furthermore, a spiking and bursting threshold is implemented. The model was tuned to reproduce bursting behavior whenever both input streams were active (as experimental data suggests, see section 3.1.4). In the absence of highly correlated inputs triggering bursts, the bottom-up input arriving at the somatic compartment showed to mainly drive the neurons activity, while the top-down input only had a modulatory effect on the total spike counts [Siegel et al., 2000].

The last compartmental model described here will also be used to confirm and tune some parameters of the pyramidal neuron model introduced in this thesis. Naud et al. 2013 used a two compartmental model of a pyramid, focussing on reproducing the spiking and bursting behaviour of pyramidal neurons in vitro.

The two compartments (somatic and dendritic) are both able to receive current input. They can interact via passively spreading APs and active propagation [Richard Naud and Gerstner, 2013].

## 3 Theory

The theoretical chapter in this thesis focuses on the latest insights into the functional properties of Layer 5 (L5) pyramidal neurons. The first section (3.1) will deal with the properties of pyramids, discussing various aspects such as the use of dendrites, the number and location of spike initiation zones and the computational possibilities resulting from the underlying functional description.

The second section (3.2) will focus on the modelling choices concerning spiking neurons, in particular on the spike response model which will be practically used. The description of the L5 pyramidal neuron model will be introduced in chapter 4. The model will be implemented and included into the latest NEST simulation environment. The possibilities and restrictions of the NEST environment will be shortly discussed in section 3.3.

### 3.1 Pyramidal Neuron Properties

This section describes some of the main properties of layer 5 pyramidal neurons. The discovery of a second spike initiation zone in pyramidal neurons, the  $Ca^{2+}$  spike, has led to a variety of new theories about the function and behaviour of pyramidal neurons.

It was further shown that the  $Ca^{2+}$  spike was unable to trigger with single dendritic input. A preceding backpropagating action potential was necessary to trigger the mechanism. This theory, named Backpropagation-activated  $Ca^{2+}$  spike firing (BAC) (3.1.1), can be explained by active dendrites, which allow the forward- and backward propagation of signals (3.1.3).

In reference to the BAC mechanism some advanced functional possibilities are discussed here, which include the internal preprocessing and coincidence detection of two information streams in a L5 pyramidal neuron (3.1.4).

### 3 Theory

The computational power of pyramids can be further enhanced by including inhibitory synaptic inputs both on distal and proximal dendrites. Some findings show that inhibitory input, especially directed between the two spike initiation zones around the oblique dendrites, can alter the functional properties of pyramids by controlling the coincidence detection mechanism and the propagation of signals along the dendritic path (3.1.5). The inclusion of a secondary spiking zone and the ability of actively propagating signals also led the way to more complex plasticity mechanisms, which are both based on Spike-timing-dependent Plasticity (STDP) and  $Ca^{2+}$ -spike triggered plasticity (3.1.6). At last the possibility of multiple spike initiation zones in distal dendritic branches is discussed (3.1.2). Figure 3.1 gives an overview of the current believed spike initiation zones in pyramidal neurons.

### 3 Theory

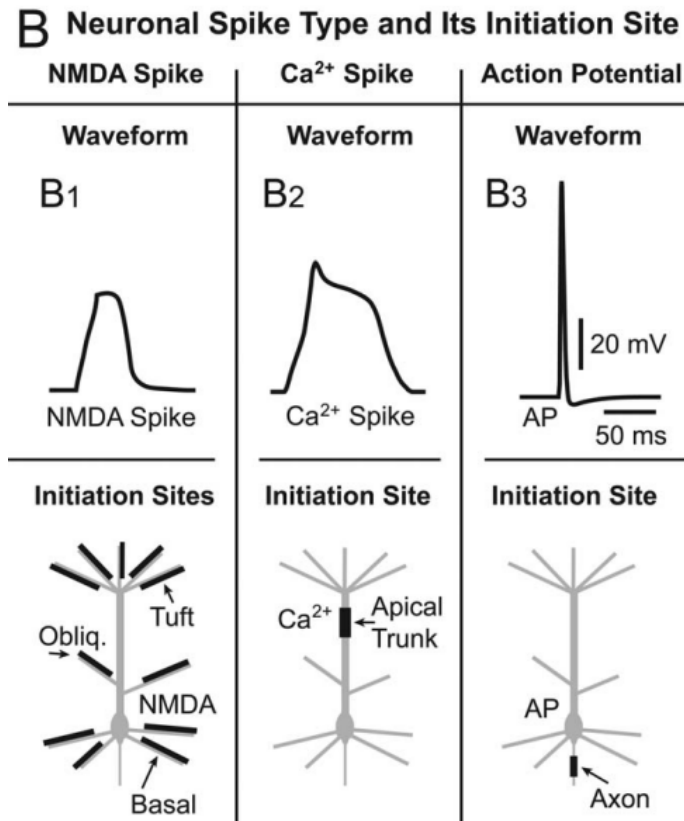


Figure 3.1: Spike initiation zones in pyramidal neurons, figure taken from [Antic et al., 2010]. The figure shows the three spike types discovered in pyramidal neurons. The NMDA and Ca<sup>2+</sup> spike are used for internal information processing, influencing the main action potential initiation zone in the axon (subplot B3 on the right). NMDA spikes (subplot B1 on the left) occur in the apical tuft, oblique and basal dendrites. They have been observed in dendrites which are below a certain diameter. The influence of the local apical NMDA spikes are summed up near the main bifurcation point in the apical trunk. In combination with a backpropagating potential from the oblique and basal synaptic inputs this can may lead to a calcium spike (subplot B2).

### 3.1.1 Calcium Spikes

The existence of dendritic calcium spikes has been widely proven in distinct classes of neurons. [Hirsch et al., 1995] showed the existence of  $Ca^{2+}$  spikes in layers 2, 3 and 5 of the cat striate cortex triggered by visual stimulation. Experiments on L5 pyramidal neurons in the rat neocortex in vitro further revealed a second spike initiation zone in distal dendrites [Schiller et al., 1997]. Moreover, the findings suggested an underlying interaction mechanism, as the initiation of the calcium spikes required the co-activation of multiple receptor channels.

[Helmchen et al., 1999] performed in vivo calcium imaging on anaesthetized rats targeting L5 pyramids. They compared their findings with L2/3 pyramidal recordings, which showed that L5 were capable of producing large  $Ca^{2+}$  transients caused by attenuated somatic currents. These transients led to immediate or delayed bursting behaviour.

[Larkum et al., 1999] later defined the term Backpropagation-activated  $Ca^{2+}$  spike firing (BAC). The experiments were performed in L5 pyramidal neurons in the somatosensory rat neocortex in vitro. They showed that  $Na^+$  action potentials initiated in the axon back-propagate into the dendritic tree, causing  $Ca^{2+}$  channels to open. In addition a current was injected into a distal dendritic branch to test a proposed coincidence mechanism between backpropagating action potentials (APs) and distal dendritic inputs.

The experiment showed no influence on the main spike initiation zone in the soma for single backpropagating axonal APs as well as for single dendritic input. However, a bursting behaviour was recorded in the main somatic spike initiation zone whenever the dendritic input was applied 3-7ms after the backpropagating potential. After 10-130ms nevertheless an inhibitory effect was reported.

The bursting behaviour was defined by the general definition of at least three APs within 20ms and less than three APs in the preceding 20ms. The coincident input triggering a  $Ca^{2+}$  spike further caused a characteristic burst pattern of 2-4 spikes at around 200Hz in the soma [Larkum et al., 2004], [Larkum, 2013]. As the dendritic calcium spike produced more action potential output as direct supra-threshold current injection into the cell body, the papers further suggested that the distal dendritic input dominates

### 3 Theory

the input/output function of the pyramidal cell. Still it could be proven that the backpropagating potential from proximal dendritic input was necessary as the threshold for calcium spikes without a backpropagating current was measured twice as high.

The existence of at least two spike initiation zones in neocortical L5 pyramidal neurons have since then been acknowledged [Ilan et al., 2011]. The paper simulated a two-compartmental model of a L5 pyramid with active dendrites. This showed that the broader  $Ca^{2+}$  spikes generate more somatic  $Na^+$  spikes than vice versa, which led to the assumption that due to synaptic plasticity the distal synapses will dominate proximal ones. However, experiments showed that the synapses are uniformly distributed along the dendritic tree [Williams and Stuart, 2002], which could only be explained by a varying degree of coupling between the two spike initiation zones (see 3.1.5).

On the contrary Stuart et al. still state that the only AP initiation zone lies in the axon. However, they acknowledge the backpropagating  $Na^+$  action potential into the dendritic tree following a spike. Also many experiments are mentioned which show the activation of  $Ca^{2+}$  channels in the dendrite. The sometimes resulting dendritic electrogenesis is considered an active form of synaptic integration rather than an action potential initiation site [Stuart et al., 1997] [Stuart and Sakmann, 1994]. Rapp et al. confirm via recordings of neocortical L5 pyramids that the only AP initiation zone lies in the axon [Rapp et al., 1996].

#### Position of $Ca^{2+}$ Initiation Zone

The exact position of the calcium spike initiation zone for neocortical L5 pyramidal neurons is still being discussed. Larkum et al. use the thick apical dendrite to measure  $Ca^{2+}$  spikes [Larkum et al., 2009]. They proclaim the calcium initiation zone to be near the apical tuft [Larkum, 2013], especially in a range between 550 and 900  $\mu m$  from the soma. The experiments were performed on rat neocortical L5 pyramids both in vitro and in vivo.

### 3 Theory

[Häusser et al., 2000] states the dendritic  $Ca^{2+}$  initiation zone to be around  $920\mu m$  from the soma. A broader range is proposed by [Perez-Garci et al., 2013] of  $600 - 900\mu m$  and [Schiller et al., 1997] of  $550 - 940\mu m$  from the soma. [Ilan et al., 2011] even suggests the  $Ca^{2+}$  spike initiation zone can extend from  $450$  to  $900\mu m$  from the soma. All experiments were carried out using in vitro slices of rat neocortical L5 pyramidal neurons. [Helmchen et al., 1999] found out that the dendritic  $Ca^{2+}$  transients were always largest proximal to the main bifurcation point of L5 pyramids.

#### 3.1.2 NMDA Spikes

Apart from the discussed secondary spike initiation zone (calcium spikes), some studies even suggest multiple spike-initiation zones along the apical dendritic tree of pyramidal neurons. [Schiller et al., 2000] performed in vitro experiments on L5 pyramids in rat sensory and motor areas. They found a proof of local AP spikes or plateaus, which were caused up to 80 per cent by N-methyl-D-aspartate (NMDA). These NMDA spikes have been recorded in the small branches of the apical tuft dendrites. The paper even suggests the possibility of dynamic spike-initiation zones, as the distribution of glutamate which depends on the ongoing activity of the neural network, can attach to NMDA receptors and therefore alter the physiology. Recently NMDA spikes were found to be initiated in the apical tuft, apical oblique and basal dendrites [Antic et al., 2010] compared to the existing sodium initiation zone in the axon and calcium initiation zone around the bifurcation area of the apical trunk.

Furthermore, a simulation was carried out using a compartmental model of a L5 pyramid from the rat somatosensory cortex [Rhodes, 2006]. The simulation results are consistent with the findings in vitro [Schiller et al., 2000]. They both proved that NMDA spikes can be initiated without the use of  $Na^+$  and  $Ca^{2+}$  currents. However, calcium and sodium currents both proved to lower the threshold of NMDA spikes. The inhibition mechanism was further compared, which showed that somatic inhibitory input had no effect on the NMDA spikes, while inhibitory dendritic input suppressed the

## 3 Theory

NMDA spike completely.

Larkum et al. also acknowledged that NMDA receptors may play a role for local computations and even suggested that NMDA spikes are the dominant mechanism by which distal synaptic input controls the firing of the neuron [Larkum et al., 2009]. The experiments implied that distal tuft dendrites are unable to support calcium electrogenesis, but are able to drive weak sodium and NMA spikes. The dendritic thickness has proven to be a good predictor of whether  $Na^+$  or  $Ca^{2+}$  ( $3.0\mu m$  and higher) electrogenesis occurs. The most recent paper [Larkum, 2013] states an in vitro experiment which concludes that NMDA spikes only affect the output of the pyramid if they are able to trigger the  $Ca^{2+}$  spike initiation zone. It is therefore suggested that some of the effects of NMDA spikes can be included into the mathematical description of calcium spikes.

### 3.1.3 Use of Dendrites

The use of dendrites is still debated. Some experiments show that distal dendritic EPSPs hardly influence the somatic membrane potential, which would suggest that EPSPs are just passively spread along the dendritic tree. Apart from that, it might be possible that the wide range of dendrites and different locations of synaptic input defines a complication that needs to be overcome by active dendritic properties, such as signal propagation (3.1.3). Finally, another possibility, which would allow dendrites to act as a preprocessor for synaptic input (3.1.3), is discussed.

#### Active or Passive

The first theory of dendritic function states that the size and shape of synaptic potentials, which reach the somatic main AP initiation site, could provide significant information about the signal source. The dendritic structure could therefore be used to act as a passive computational subunit, where passively spread EPSPs influence each other according to the structural

### 3 Theory

design of the dendrite [Häusser et al., 2000].

The second theory completely ignores the dendritic structure and states the different locations of synaptic inputs along the dendritic tree as an obstacle that needs to be overcome. By choosing active dendrites (presence of propagating  $Na^+$  and  $K^+$  currents) the distance to the soma does not matter [Destexhe and Pare, 1999]. This would line up with the point-neuron hypothesis, where all synaptic inputs are equally integrated [Häusser and Mel, 2003]. There exist also experiments which show the active properties of dendrites. Neocortical L5 pyramids have proven to possess active  $Na^+$  channels all along the apical dendrite, while hippocampal L5 pyramids show a distribution of active Sodium channels from the apical dendrite until around  $200\mu m$  from the soma [Stuart and Sakmann, 1994].

#### Information Processing Capabilities

Apart from the active properties of the dendrites, there exist many theories about the computational power. Häusser et al. proposed that the dendritic tree should be compartmentalized based on voltage-gated ion channel densities and the synaptic activation pattern. The different compartments can further take over the integration of synaptic input [Häusser et al., 2000]. [Polsky et al., 2004] provides experimental evidence (L5 neocortical rat pyramidal neurons, *in vitro*) showing that thin dendrites act as computational subunits, which sum up synaptic input using a sigmoid kernel function. They found out that nearby inputs are summed up sigmoidally while spatially further distributed inputs are summed up linearly. This led to an incompatibility with a global summation rule as proposed by the point neuron hypothesis. In order to conform with the experimental data, a two-layer neural network is necessary.

Larkum et al. also acknowledged that thin distal tuft dendrites, which receive the majority of synaptic inputs, as well as basal dendrites sum up synaptic input with the use of NMDA spikes. The output of these computational subunits is passed on via actively propagating signals to one of the two main synaptic integration sites, namely the axonal  $Na^+$  spike initiation site and the apical  $Ca^{2+}$  initiation site [Larkum et al., 2009].

## 3 Theory

The findings have further been confirmed by [Spratling, 2002], who states that the apical dendrite has to act as a separate compartment, and [Xu et al., 2012] performed an in vivo experiment on mice tracking L5 pyramids in the barrel cortex, an area of the somatosensory cortex associated with facial whiskers of rodents [Manns et al., 2004]. They proved that the dendrites actively integrate and process input.

However, [Behabadi and Mel, 2014] question the independence of dendritic computational compartments as experimental data showed that backpropagating potential from the soma resets the membrane potential in dendrites. They developed a two layer neural network from the example in [Polsky et al., 2004], where the first layer consists of multiple independent dendritic subunits, which use a non-linear input output function. The second layer sums up the dendritic output and produces an output based on the cells somatic firing-rate to current curve. Even though no backpropagating effects have been applied to the simulation, the model still outperforms passive dendritic models in predicting pyramidal neuron responses. As an explanation they enlisted the possibility that pyramidal cells specialized in minimizing the disruptive effects of backpropagation-mediated cross-talk between dendritic subunits which would allow multiple dendritic compartments to perform computations individually [Behabadi and Mel, 2014]. The implementation of a model with two sites of synaptic integration has also been tested [Körding and König, 2001]. They showed that their neuron model can implement learning principles of spatial and temporal continuity, as used in image processing.

### 3.1.4 Coincidence Detection

The existence of active dendrites with information processing capabilities, as discussed in the preceding sections (3.1.3 and 3.1.3), leads to a variety of possibilities in which way to combine the two information streams and how to make use of the enhanced computational properties of a neuron with two independent sites of synaptic integration.

Siegel et al. lined out various anatomical and psychophysical studies which show that top-down effects (or feedback signals) play an important role in

### 3 Theory

the processing of sensor (feedforward) information [Siegel et al., 2000]. The source and target layer of pyramidal neuron axons is used as a classifier for feedforward and feedback streams in the cortex [Spratling, 2002]. This suggests that sensory driven or feedforward input arrives at the basal dendrite, while top-down or feedback information is fed to the apical dendrite. Spratling et al. further outline some possibilities of how to combine the two information streams. The simplest form called *Reconstruction* handles the two information streams equally. Both basal and apical input can trigger the output spikes of the neuron, so the feedback stream can be used to reconstruct sensory data when it is temporary unavailable.

*Modulation*, the second theory, handles the feedback signal as an amplifier signal, which is able to enhance sensory data that matches the top-down expectation and suppress data that is unexpected.

Finally, *Suppression* describes the vice versa principle of *Modulation*, and could be used to filter the sensory input signal with the use of feedback information so that only unexpected and new information is passed on. This principle could also be used to provide error information or supervision for learning at the basal synapses.

[Larkum, 2013] supports the *Modulation* theory in a more abstract way, using the feedback stream as a predictor whether the neuron should fire or not. The firing nevertheless is modulated by the feedforward input. Larkum et al. defined the location of the coincidence detection in the dendritic compartment with a coincidence time of 20-30ms between distal dendritic EPSPs and the backpropagating potential from the soma. The BAC mechanism is therefore proposed as another mechanism for gain modulation. As the passive influence of synaptic inputs on the soma decreases with rising distance, the gain modulation caused by the backpropagating signal ranges from 22% to 72%, being highest at the most distal dendritic input locations [Larkum et al., 2004].

Figure 3.2 shows an example of the three mentioned ways of combining two information streams in neurons.

### 3 Theory

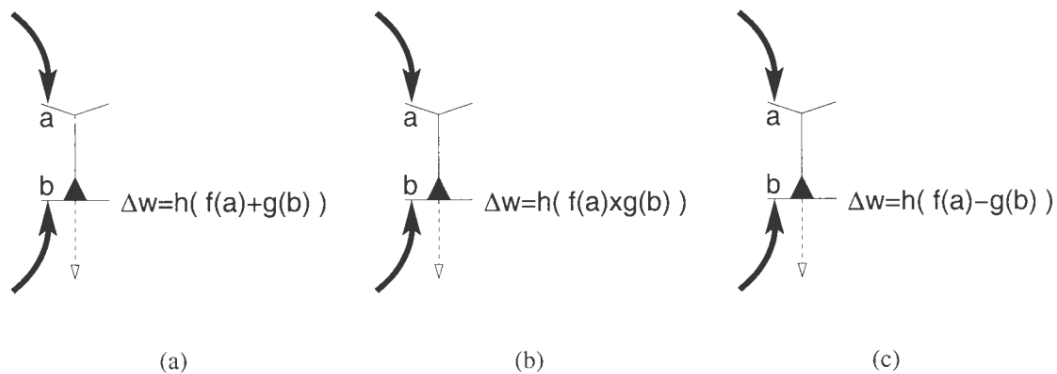


Figure 3.2: Concept of three possible ways to combine two information streams, *Reconstruction* a), *Modulation* b) and *Suppression* c). Figure taken from [Spratling, 2002]. Plot a) shows the *Reconstruction* principle, where the two input streams (a and b) were both summed up to produce the output function. Taken into account that only one of the two input streams is active at the same time, one input stream can be used to reconstruct the output behaviour if the other stream is missing. Plot b) shows the *Modulation* principle, where both input signals are multiplied. One of the streams can therefore be used to modulate the other one, changing the amplitude (influence) of the input signal. Plot c) at last shows the *Suppression* principle, where the second input stream (b) is subtracted from the first input (a). This principle can be used for error calculation, where an output is only produced if the two signals do not match.

Other experiments confirmed the 30ms coincidence time window between apical and basal input [Sjöström and Nelson, 2002] [Major et al., 2013]. In addition the duration of a burst caused by simultaneously active input streams also lasts around 30ms, which may incline that this time scale has a special significance in the neocortex.

However, [Major et al., 2013] showed that the coincidence time window can be altered (see section 3.1.5) by the location and activity of apical oblique dendrites.

#### 3.1.5 Inhibition & Coupling

Many experiments and computer simulations show that synaptic inhibition, either specifically targeted or due to normal background activity, can alter

### 3 Theory

the signal propagation properties of  $Na^+$  and  $Ca^{2+}$  currents in the dendritic tree of pyramidal neurons [Häusser et al., 2000]. Rapp et al. showed that background synaptic activity alone changes the backpropagation of somatic APs. This behaviour can only be tested *in vivo*, which could be done using whole cell recordings in neocortical L5 rat pyramidal neurons. They showed that a background activity of 1.5Hz led to a decrease of 15% of the backpropagating somatic potential measured 550 $\mu m$  from the soma. 3Hz background activity led to 27% decrease [Rapp et al., 1996].

Experiments further tested the effect of specifically located IPSPs on the somatic potential. Pare et al. showed via *in vivo* experiments on neocortical cat pyramids and computer simulations that proximal IPSPs prevented  $Na^+$  currents in the dendrite from interfering with the somatic membrane potential and even reduced the amplitude and duration of somatic spikes [Pare et al., 1998]. [Gerstner and Kistler, 2002] also showed that inhibitory input spikes are able to shunt information from reaching the soma. If located in specific locations (see section 3.1.5) a few input spikes were able to shunt input which was gathered by hundreds of excitatory dendritic synapses. Nevertheless, other experiments showed that inhibitory postsynaptic potentials were able to reduce the amplitude of distal dendritic spikes, while they were not altering the amplitude of APs in somatic or proximal dendritic regions [Tsubokawa and Ross, 1996]. It was therefore proposed that inhibitory inputs just affect the backpropagating APs from the soma, changing actively propagated signals to passively spreading potentials. The inhibition showed to be most effective when evoked during a time window of less than 10ms after a somatic spike.

The influence of inhibitory signals on  $Ca^{2+}$  spikes have further been focused on. Self-initiated calcium spikes, which resulted without former backpropagating potential from the soma and which could get inhibited by inhibitory interneurons [Ilan et al., 2011], have been reported. Kim et al. also showed that IPSPs were able to delay and partially or fully block dendritic spikes, as was tested *in vitro* in somatosensory L5 rat pyramids [Kim et al., 1995]. Similar experiments also acknowledged that inhibitory inputs on the apical trunk are able to delay or suppress dendritic  $Ca^{2+}$  APs, while they do not influence proximal dendritic regions or the soma. They are therefore

### 3 Theory

proposed to simply decouple the input streams and suppress the active propagation up to 400ms [Larkum et al., 1999] [Helmchen et al., 1999].

#### Effective Location for Inhibitory Input

The differences between inhibitory inputs targeting the soma and dendrites of pyramids have been examined. Miles et al. show that only dendritic inhibitory inputs are able to suppress the generation of calcium-dependent APs. However, the experiment was carried out using CA3 pyramidal neurons [Miles et al., 1996]. Besides an in vitro experiment on L5 pyramids in rat somatosensory cortex revealed that inhibitory signals targeting the soma suppress dendritic spikes as well as dendritic inhibitory inputs. The in vitro study in combination with the simulation of a detailed compartmental model showed that dendritic IPSPs influence the threshold of the dendritic spike, while somatic IPSPs alter the amplitude of the calcium spike. This behaviour is suggested to multiply the computational power of inhibitory interneurons, as cortical circuits can therefore alter threshold and gain of dendritic spikes individually [Jadi et al., 2012].

The most prominent location for inhibitory signals to connect to pyramidal L5 neurons has proven to lie in the proximal dendritic region. Stuart et al. have already mentioned that most inhibitory synapses have to connect close to the soma to have the greatest influence on the somatic membrane potential [Stuart et al., 1997]. This was acknowledged and specified to a region from the soma to about  $400\mu m$  from the soma [Gerstner and Kistler, 2002] [Larkum et al., 2001].

Häusser et al. also proposed that the coupling between the somatic and the dendritic spike initiation zone depends on the oblique dendrites [Häusser and Mel, 2003], a view which was proven through experiments and simulation by [Schaefer et al., 2003]. The experiments further showed that the geometry of proximal and distal oblique dendrites originating from the main apical dendrite determine the degree of coupling between the spike initiation zones. Oblique dendrites originating at a distance of over  $140\mu m$

## 3 Theory

from the soma have shown to decrease coupling, while oblique dendrites closer by increased it.

### 3.1.6 Plasticity

The first section deals with theories concerning the use of synaptic plasticity in the neocortex (3.1.6). The subsequent sections will describe different theories about the reasons for synaptic plasticity in L5 pyramids. The complex functional structure of pyramidal neurons leads to a variety of possible plasticity controlling factors, such as the backpropagating somatic potential and the  $Ca^{2+}$  spike and its intrinsic firing rate (3.1.6).

#### Use of Plasticity

Sourdet et al. [Sourdet and Debanne, 1999] mentioned that synaptic plasticity changes are thought to be the fundamental mechanism underlying the creation of persistent memory in the brain. The Hebbian learning principles, including long-term potentiation and depression (LTP and LTD) have been verified in neocortical and hippocampal pyramidal neurons, while non-pyramidal neurons have shown different results.

Markram et al. announced another theory saying that synaptic plasticity is not only used for learning, but also represents the main information processing mechanism in neocortical neural networks [Markram et al., 1998]. Due to mathematical analysis of the synaptic transfer function they found a range of different possible functions depending on the linear representation of the pre-synaptic firing rate as well as on the integral and differential. As the synaptic plasticity can be changed individually, it is likely that a single axon is distributing different features of a propagating spike train towards different target neurons. The study further predicts that AP activity patterns transmitted over an axon can change the synaptic transfer function individually. This would lead to a different representation of the AP pattern at the synapse, making iterations of synaptic transfer functions possible.

While the occurrence of both depressing and facilitating synapses on one axon depending on the pre- and postsynaptic neuron has been extensively studied in between interneurons and L5 pyramidal cells, another study

### 3 Theory

suggests that this also occurs in between pyramids [Wang et al., 2006]. The study has been carried out in vitro using slices of the medial prefrontal cortex of adult ferrets.

#### Backpropagation as a Source for Plasticity

Sjöström et al. are reviewing the potential effects of EPSPs in addition to backpropagating postsynaptic APs for plasticity. To change dendritic synapses, the AP initiated in the axon has to be backpropagated into the dendritic tree [Sjöström and Nelson, 2002]. The influence of backpropagation was furthermore acknowledged [Häusser et al., 2000] and it was also proclaimed that backpropagating APs could serve as a global rather than as a local signal for synaptic plasticity [Paulsen and Sejnowski, 2000].

Häusser et al. lined out a different view where the spatial extent of propagation is a varying and determining factor for the range of plasticity. This would conclude that depending on the structure of dendrites and the momentary synaptic activity on the way, which influences the propagation abilities, different parts of the dendritic tree would be invaded by the preceding axonal spike [Häusser and Mel, 2003].

Another theory suggests that dendrites can influence their plasticity individually. Synapses at  $< 450\mu\text{m}$  from soma, in the paper called “proximal” use the somatic  $\text{Na}^+$  spike as their STDP inducing signal, while “distal” synapses use the  $\text{Ca}^{2+}$  spike [Ilan et al., 2011]. Körding also showed that the triggering of calcium spikes could lead to LTP [Körding and König, 2000].

The implications of spreading depolarization and propagating APs on synaptic plasticity have also been reviewed by Sourdet et al. [Sourdet and Debanne, 1999]. Long-term potentiation (LTP) was shown to occur whenever a postsynaptic backpropagating AP is paired with preceding pre-synaptic stimulation in a time window of 50 to 240ms. However, these findings have been refined as Debanne et al. showed that LTP is only induced if a burst of 10 to 12 postsynaptic backpropagating APs is encountered in a time window of 240ms. A burst of three to four APs showed no significant effect on plasticity while single APs could even result in LTD if the time delay

## 3 Theory

between the post- and pre-synaptic activity is around zero ([Sourdet and Debanne, 1999], Figure 2A,D).

The importance of rate over timing, as traditionally thought of STDP, was also acknowledged by [Sjöström and Nelson, 2002], who lined out that multiple APs are needed to allow LTP for low frequencies. Paulsen et al. further showed through in vitro experiments in adolescent and adult rat and mice hippocampal pyramids that the pairing of single pre- and postsynaptic APs for the induction of LTP or LTD is only sufficient in premature animals. Adult animals require postsynaptic bursts to induce LTP [Paulsen and Sejnowski, 2000].

In contrast to burst-triggered LTP, Bi et al. [Bi and Poo, 1998] showed that single postsynaptic APs require a very short coincidence time window of 20ms to induce LTP. This result was already proclaimed by [Sourdet and Debanne, 1999], who proposed that single APs would require a higher temporal sensitivity than bursts.

## 3.2 Neuron Modelling

### 3.2.1 Spike Response Model

In the practical part of this thesis the spike response model [Scholarpedia, 2014] will be used to describe the pyramidal neuron model. The spike response model (SRM) is a generalization of the integrate-and-fire (IAF) model. While the IAF neuron is described by differential equations, the SRM is formulated using filters. Furthermore, the SRM can include a refractory period.

In models such as the spike response model or the integrate-and-fire model, neurons are viewed as units which sum up postsynaptic potentials resulting of presynaptic spikes and generate a spike if a given threshold is reached. A more advanced version of the IAF model, the leaky integrate and fire model, which includes a term mapping the diffusion of ions through the membrane over time causing a decay in membrane potential, has been proven to provide a good representation of in vitro recordings of L5 pyramidal neurons,

### 3 Theory

for instance from sensorimotor cortex of adult rats in vitro [Paninski et al., 2003].

There have also been a few theoretical and practical studies concerning the issue of whether different forms of the spike response model representation can account for the complexity of biological neurons. Jolivet et al. performed a study using recordings of L5 pyramidal neurons from rat somatosensory cortex in vitro. The neurons were stimulated using a fluctuating current. These experimental results were compared to a simple SRM, where up to 75% of the recorded spikes could be reproduced and predicted with a time precision of +/- 2ms [Jolivet et al., 2006].

Furthermore, the SRM has been compared to other theoretical models describing neurons. In a study by Kistler et al., the SRM has been compared to a hodgkin-huxley representation, where over 90% of the spikes could be reproduced using a stochastic input current [Kistler et al., 1997]. The model was also compared to a conductance-based model, as the study showed that a simple conductance-based model can be easily reduced to a threshold model representation, such as the leaky integrate-and-fire model with an exponentially rising spiking current depending on the input frequency or the SRM [Fourcaud-Trocme et al., 2003].

#### 3.2.2 Stochasticity

The role of stochasticity in neuronal modelling is also still being discussed. Today most simulations use some kind of stochasticity, while others argue that stochastic terms should be removed, as they are only representations of nonlinear varying factors such as response saturation which might be exploited [Paninski et al., 2004].

In general, two sources of noise are believed to exist for biological neurons. Intrinsic noise is created by a stochastic release of neurotransmitters and the resulting stochastic opening and closing of some ion channels. External noise sources are regarded as random network activity, represented as stochastic spiking input from other neurons. Usually, only the external noise is modulated by using a poisson input current in addition to the target

signal [Burkitt, 2006].

It has also been shown that a noisy threshold mechanism can account for much of the unexplained unreliability and variability of biological neurons [Jolivet et al., 2006]. Therefore, as further detailed information about the intrinsic properties of neurons are missing, stochasticity provides a good representation of otherwise unaccounted biological effects.

### 3.3 NEST Simulation Environment

As experimental studies imply that the neural activity of the brain is observed using either only a few neurons via intracellular recording techniques such as voltage clamp or patch clamp or a wide range of neurons (up to  $10^6$ ) by large-scale recording techniques such as electroencephalography (EEG), functional magnetic resonance imaging (fMRI) or positron emission tomography (PET) [Buzsaki, 2004].

Theoretical and computational models are therefore required to interpolate the missing information and predict neuron states. As information processing is believed to rely mostly on action potential changes and neuronal spikes, many simulation techniques have emerged which focus on the simulation of spiking neuron models [Brette et al., 2007].

In the practical part of this thesis the Neural Simulation Technology (NEST) is used to simulate the pyramidal neuron behaviour. The NEST simulator is an open source application built to simulate large networks of heterogeneous elements. It allows biologically realistic neuron models and neuronal networks to be implemented on different levels of abstraction. While most spiking neuron simulation tools use a bottom-up concept, mainly focusing on the modelling and simulation of single neuron models, NEST uses a top-down approach. This approach allows a network to be described using abstract components, which can consist from single synaptic models or one compartment of a neuron to a whole subset of neurons. The simulation environment therefore makes the generation of a hierarchical structure easy, where functional related neurons can be grouped together forming an abstract component [Diesmann and Gewaltig, 2001]. Furthermore, NEST is

### 3 Theory

built as a research tool, allowing flexible and easy adaptation of components as new theoretical information gets available.

The components are designed using the object-oriented programming language C++. The object-oriented approach especially makes different levels of abstraction possible. Based on an abstract core class [Diesmann and Gewaltig, 2001], all components need to implement specific methods and basic functionality. As described later in this section the computation itself is also handled in the component class, which allows different representations of theoretical theories (for example, differential equations) to be implemented in one simulation network. However, each component is restricted, for example, each model can only send a single type of predefined event, either spike event, current event, rate event or potential event. Even so, they are able to receive several events from other components, which can be applied repeatedly using different input channels. This can, for instance, enable the attachment of different synaptic models with different behaviours (facilitating or depressing) but one comprehensive event to a component [Initiative, 2014].

In addition to the biologically inspired components, some abstract modules are available, representing random number generators, signal generators for currents, voltages and measurement tools such as spike detectors.

All components are hard-coded and compiled preceding a simulation. C++ is used to retain the best possible performance [Brette et al., 2007].

For the simulation itself a proprietary language called Simulation Language Interpreter (SLI) is used. The main reason for using SLI is its support for heterogeneous arrays. In contrast to C++, where memory management is a major issue, SLI makes the assignment and maintenance of size-varying data structures easy and efficient [Diesmann and Gewaltig, 2001]. In contrast to an event-driven simulation, where a supervising scheduler is collecting and queuing event, NEST uses a time-driven simulation approach, where events (for example, spikes) are sent out and queued at the target neuron [Brette et al., 2007]. This time-driven approach is especially useful for large number of connections to simple components, as it allows a decentralized memory organization without the need of a scheduler to queue, send and

### 3 Theory

allocate events for thousands of target neurons.

SLI furthermore uses an internal dictionary structure and keyword parameters in order to access and modify model parameters. This enables an easier user interface where just two methods, which need to be implemented by all abstract components, are required to modify a model [Diesmann and Gewaltig, 2001].

The connections between components are also defined in the simulation environment, allowing convergent, divergent, random and topological connections to be implemented. Moreover, an additional delay, weight or whole synaptic transfer model can be applied [Initiative, 2014]. The connections are also checked for consistency at the time of creation.

In addition there exist a few programming language interfaces such as python, which is used in this thesis, to access SLI commands.

Today the simulation of  $10^4$  neurons is common using NEST. Although  $10^5$  were already simulated using the simulation environment, this was only possible by using external parallelization tools such as a Message Passing Interface (MPI), which distributes the computation tasks along multiple workstations of a cluster. A future release of NEST is planned to natively contain multi-threading and message passing interfaces to allow larger neural networks being simulated. If  $10^5$  neurons can be simulated, the volume of the cortex can be represented in a biologically realistic manner, without the need of downscaling synaptic connections or neuron complexities [Diesmann and Gewaltig, 2001].

## 4 Concept

This chapter deals with the development of a design and simulation concept for a L5 pyramidal neuron model. The first section (4.1) outlines the requirements for the neuron model (4.1.1) and compares the model to its biological prototype (4.1.2). After that, the mathematical basis for the compartmental model is derived (4.1.4). The second section (4.2) reformulates the model into a hidden Markov model and outlines a simulation concept to automatically retrieve some hidden model parameters.

### 4.1 Pyramidal Neuron Model

#### 4.1.1 Requirements

The pyramidal neuron model developed in this thesis will be described using the spike response model formalism [Scholarpedia, 2014]. For a short introduction and explanation of this choice see section 3.2.1.

The model should further consist of four compartments, which divide the neuron into three main dendritic input areas, namely an apical, an oblique and a basal input area. Moreover, the soma will be described as a separate compartment. The somatic and apical compartments will contain the two main spike initiation sites, as predicted by theoretical results (see section 3.1.1). The description of more than two spike initiation sites (see section 3.1.2) will be omitted in this thesis for reasons of brevity.

The propagation mechanism in between the compartments is modelled by a low pass mechanism. The oblique dendritic compartment can be used to influence this propagation mechanism via inhibitory inputs (see section

## 4 Concept

3.1.5 for explanation).

The model should also contain a stochastic firing mechanism based on a simple exponential function as proposed by [Jolivet et al., 2006]. In addition to an overlaid poisson input signal, this mechanism accounts for some unreliable biological effects of pyramids as described in section 3.2.2.

### 4.1.2 Simplifications

In this section, a few of the applied simplifications of the pyramidal neuron model in comparison with its biological realistic counterpart are listed.

First of all, no spatial differences in dendrites are taken into consideration. Apart from the compartmentalization into four main regions, no differences in synaptic location are recognized. Nevertheless, this modelling principle is conform with some theoretical and experimental results which decline the effects of spatial differences in synaptic inputs [Häusser et al., 2000] [Destexhe and Pare, 1999].

As already described in section 4.1.1, only three main synaptic integration sites (basal, apical and oblique dendritic compartments) and two spike initiation sites (apical and somatic) are considered. As suggested by Larkum et al. some experimental findings show that NMDA spikes are only used to distribute the spatially distributed dendritic EPSPs and that their influence can be included in the mathematical formalization of the dendritic calcium spike [Larkum, 2013].

Although the synaptic plasticity is modelled using a rate-based learning algorithm (see section 5.4.4 in chapter 5), no spike-timing-dependent plasticity (STDP) is used in this thesis. Additionally according to recent theoretical results the synaptic plasticity does not only depend on spike-timing-dependent plasticity (STDP), but also on the propagation properties of neurons. In the distal dendritic compartment long-term potentiation (LTP) is believed to rely on the backpropagating potential from the soma [Häusser et al., 2000] [Körding and König, 2001] [Paulsen and Sejnowski, 2000]. Other findings indicate that LTP in the apical dendrite is induced by  $Ca^{2+}$  spikes, while LTP in dendrites proximal to the soma use  $Na^+$  spikes as their main

## 4 Concept

source of plasticity [Ilan et al., 2011]. However, as the backpropagating current is modelled and already considered in the dendritic synaptic integration sites, the influence of backpropagation can be easily added to the existing model described here.

### 4.1.3 Model Schematic

In this section the main schematic of the model with input- and output-streams is printed. Figure 4.1 shows a typical sketch of a pyramidal neuron taken from [Sjöström et al., 2008] and the separation of the neuron into four major compartments. The compartment separation is based on its biological behaviour, mapping the soma and the apical, oblique and basal dendrites separately. The compartments are later referred to based on their capital letter (A for apical compartment, B for basal, O for oblique and S for somatic). Figure 4.1 on the right shows the abstract representation of the neuron model with the input currents arriving at the two main integration sites (input stream  $a$  arrives at the apical compartment, responsible for calcium spike integration and input stream  $b$  arrives at the basal compartment). The input stream for oblique dendrites has been omitted for simplicity. Nevertheless, it is implemented in the model and can be used in a subsequent simulation.

Furthermore, the abstract representation holds the propagating currents, namely  $u_A^{FP}$  representing the forward propagating action potential from the apical to the somatic compartment and  $u_S^{BP}$  representing the backpropagating potential from the soma.

#### 4 Concept

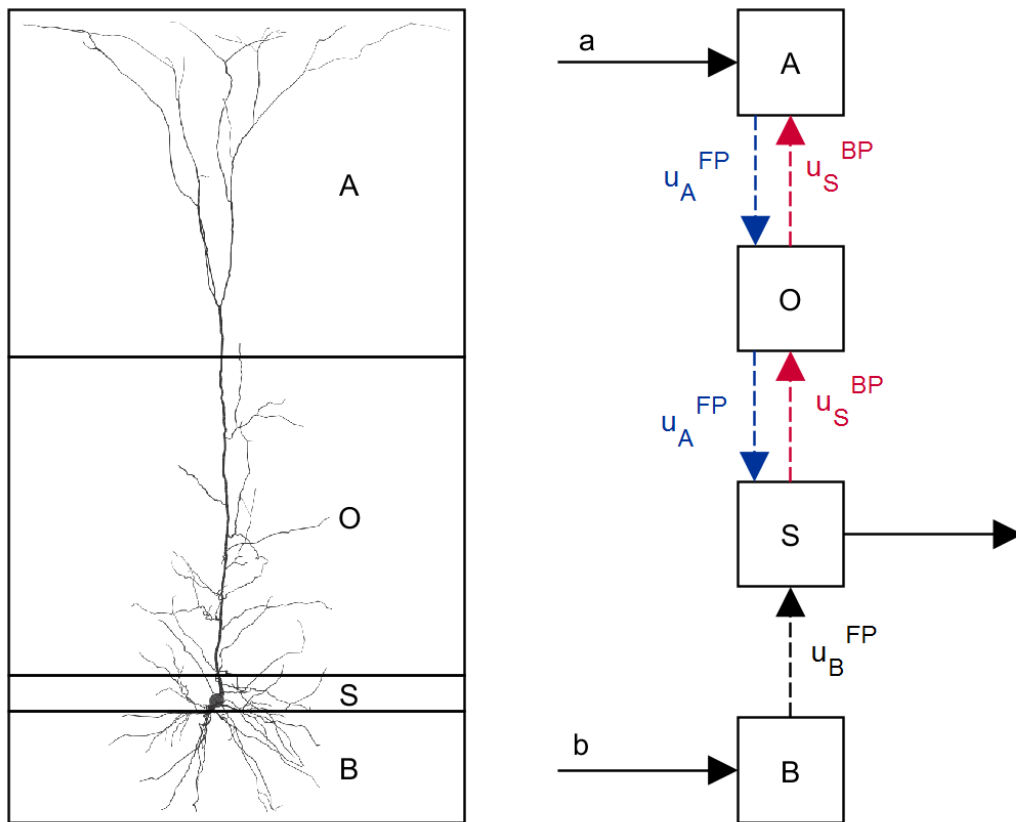


Figure 4.1: Conceptual L5 pyramidal neuron model. The neuron drawing was taken from [Sjöström et al., 2008]. The neuron was divided into four compartments. The A(pical) compartment is able to receive synaptic inputs (a). The apical membrane potential  $u_A^{FP}$  is then propagated through the O(blique) compartment to the S(omatic) compartment. The B(asal) dendritic compartment on the bottom is also able to receive synaptic input (b) and the basal membrane potential  $u_B^{FP}$  also propagates into the somatic compartment. The soma then combines the two potentials and triggers an output spike whenever a stochastic threshold is reached. Additionally the somatic membrane potential  $u_S^{BP}$  is back-propagated into the A(pical) compartment, which may trigger a calcium spike.

#### 4.1.4 Model Description

This section describes the mathematical basis of the model. It is divided into four subsections, each dealing with one of the major compartments as outlined in figure 4.1.

The effects of the various propagating potentials can be best overviewed by the simulation comparing the pyramidal neuron model with the Larkum experiments (see section 5.4.1).

##### Distal Apical Dendritic Compartment (A)

The distal apical dendritic compartment, abbreviated as A, sums up the EPSPs of the apical dendritic tree. The postsynaptic potentials are summed up linearly depending on the  $\epsilon_A$  kernel modelling the time course of the EPSP.

Furthermore, the backpropagating somatic membrane potential ( $u_S^{BP}$ ) is added to the membrane potential. The membrane potential  $u_A$  therefore lines up to:

$$u_A(t) = u_{rest} + \sum_a w_a \sum_f \epsilon_A(t - t_a^f) + u_S^{BP}(t) \quad (4.1)$$

In equation 4.1 the EPSP time course ( $\epsilon$ ) is summed up over all presynaptic spikes  $f$ . It is afterwards multiplied with the synaptic weight  $w_a$  and summed up again over all apical synapses. Additionally the backpropagating membrane potential from the somatic compartment  $u_S^{BP}$  is added.

The EPSP time course is given by:

$$\epsilon_A(\Delta t) = \Delta t \cdot e^{\left(\frac{-\Delta t}{\tau_{Rise}}\right)} \quad (4.2)$$

A single exponential is used as the low pass function for the somatic membrane potential propagating from the somatic to the apical dendritic

## 4 Concept

compartment:

$$u_S^{BP}(t) = u_S \cdot \gamma_{S-A}(t) \quad (4.3)$$

Where the  $\gamma$  kernel describes the low pass characteristic between the S(omatic) and the A(pical) compartment (S-A):

$$\gamma_{S-A}(t) = \left(1 - e^{\left(\frac{-t}{\tau_{S-A}}\right)}\right) \quad (4.4)$$

The role of the parameters are summarized in table 4.1.

$a$	presynaptic neurons connected to the apical compartment
$\epsilon_A(t - t_a^f)$	time course of the response to an incoming spike f
$u_S^{BP}(t)$	backpropagating (BP) potential from the somatic compartment
$\tau_{Rise}$	rise time for the activation function applied to the synaptic efficacy, can be different for each compartment
$\tau_{S-A}$	lowpass time constant between S(omatic) and A(pical) compartment

Table 4.1: Variables used in the apical dendritic compartment representation

### Oblique Dendritic Compartment (O)

In accordance with the theoretical findings of oblique dendrites to act as regulators for back- and forward-propagation and inhibition (section 3.1.5) the oblique dendritic compartment, abbreviated as O, is used to change the low pass function of the backpropagating somatic membrane potential  $u_S^{BP}$  and the forward propagated apical membrane potential  $u_A^{FP}$ .

In order to determine which low pass function should be used, the compartment needs to sum up its inhibitory synaptic input. The resulting membrane

## 4 Concept

potential is calculated as follows:

$$u_O(t) = u_{rest} + \sum_o w_o \sum_f \epsilon_O(t - t_o^f) \quad (4.5)$$

If the inhibitory synaptic input reaches a certain threshold  $\vartheta_O$  the propagating voltages are low pass filtered using a different time constant  $\tau_{x-y}^{Inh}$ . Therefore, if  $u_O(t) > \vartheta_O$  the following equations hold:

$$u_S^{BP}(t) = u_S \cdot \gamma_{S-A}^{Inh}(t) \quad (4.6)$$

$$u_A^{FP}(t) = u_A \cdot \gamma_{A-S}^{Inh}(t) \quad (4.7)$$

With  $\gamma^{Inh}$  as follows:

$$\gamma_{S-A}^{Inh}(t) = \left( 1 - e^{\left( \frac{-t}{\tau_{S-A}^{Inh}} \right)} \right) \quad (4.8)$$

$$\gamma_{A-S}^{Inh}(t) = \left( 1 - e^{\left( \frac{-t}{\tau_{A-S}^{Inh}} \right)} \right) \quad (4.9)$$

The role of the parameters are summarized in table [4.2](#).

## 4 Concept

$o$	presynaptic neurons connected to the oblique compartment
$\epsilon_O$	time course of the response to an incoming spike
$\vartheta_O$	stochastic threshold
$u_S(t)$	membrane potential of the soma
$u_S^{BP}(t)$	backpropagated (BP) membrane potential from the somatic compartment to the apical (A) compartment
$u_A(t)$	membrane potential of the distal dendritic compartment (A)
$u_A^{FP}(t)$	forward-propagated(FP) membrane potential from the distal dendritic compartment (A) to the soma (S)
$\tau_{S-A}^{Inh}$	lowpass time constant between somatic and apical compartment during inhibitory input
$\tau_{A-S}^{Inh}$	lowpass time constant between A(pical) and S(omatic) compartment during inhibitory input

Table 4.2: Variables used in the oblique dendritic compartment representation

### Somatic Compartment (S)

The somatic compartment acts as the main spike initiation site. It receives input from all other dendritic compartments and combines the propagated voltages.

The somatic membrane potential consists of the propagating apical membrane potential ( $u_A^{FP}$ ) and the propagating basal membrane potential ( $u_B^{FP}$ ). The oblique membrane potential  $u_O$  is not considered in the formula as it already influences the potential by changing the propagation mechanism to and from the apical compartment.

$$u_S(t) = u_{rest} + u_A^{FP}(t) + u_B^{FP}(t) + \eta_{BAC}(t - \tilde{t}) + \eta_S(t - \hat{t}) \quad (4.10)$$

## 4 Concept

The term  $\eta_S$  is the so called response kernel, describing the form of the somatic membrane potential after a spike was created.  $\eta_{BAC}$  describes the form of the backpropagating calcium spike at the soma respectively.

Usually, the calcium spike is triggered in the apical dendrite, as discussed in section 3.1.1. However, in this mathematical representation there is no difference if the calcium spike is created in the apical compartment and propagates into the soma, or if the propagating membrane potential from the apical compartment is used to trigger an abstract representation of the calcium spike influence in the soma. This second principle is used here. The propagated apical dendritic membrane potential  $u_A^{FP}$  is compared to the threshold value  $\vartheta_{BAC}$ . In case the threshold is exceeded  $\tilde{t}$  is set to  $t$ , marking the starting point of the calcium spike and the calcium spike response kernel  $\eta_{BAC}$  is initialized.

$\eta_{BAC}$  is modelled by a rectangular pulse, followed by a fixed refractory period. During the pulse time the somatic membrane potential is set above the  $Na^+$  threshold level, triggering a burst of APs.

$$\begin{aligned} \text{If } u_A^{FP}(t) > \vartheta_{BAC} : \\ \tilde{t} = t \end{aligned} \quad (4.11)$$

$$\begin{aligned} \text{For } \tilde{t} < t < \tilde{t} + \Delta_{dead} : \\ \vartheta_{BAC} = \infty \end{aligned} \quad (4.12)$$

Equation 4.11 describes the refractory period of the BAC firing mechanism. After the ignition of the calcium spike at time  $\tilde{t}$  the threshold for triggering another calcium spike  $\vartheta_{BAC}$  is set to infinity until the refractory period  $\Delta_{dead}$  is over.

The sodium spiking mechanism, which serves as the output function of the pyramidal neuron is triggered if the somatic membrane potential  $u_S$  exceeds the threshold value  $\vartheta_S$ . In order to account for unreliable biological effects, a stochastic threshold following a single exponential is used.

$$p(\text{spike}) \propto e^{\alpha_{Norm} \cdot (u_S(t) - \vartheta_S)} \quad (4.13)$$

## 4 Concept

The influence of the sodium spike on the somatic membrane potential  $\eta_S$  and the following refractory period is modelled as follows. In these formulas  $\hat{t}$  marks the position of the sodium spike:

$$\eta_S(t - \hat{t}) = -\vartheta_S \cdot e^{\left(\frac{\hat{t} - t}{\tau}\right)} \quad (4.14)$$

For  $\hat{t} < t < \hat{t} + \Delta_{dead}$  :

$$\vartheta_S = \infty \quad (4.15)$$

The following equations describe the form of the propagating voltages from the dendritic compartments. If oblique dendritic inputs are desired, the inhibitory effects may change the low pass function of the propagating potential from the apical compartment, as described in section 4.1.4.

$$u_A^{FP}(t) = u_A \cdot \gamma_{A-S}(t) \quad (4.16)$$

$$u_B^{FP}(t) = u_B \cdot \gamma_{B-S}(t) \quad (4.17)$$

With the respecting low pass kernela as follows:

$$\gamma_{A-S}(t) = \left(1 - e^{\left(\frac{-t}{\tau_{A-S}}\right)}\right) \quad (4.18)$$

$$\gamma_{B-S}(t) = \left(1 - e^{\left(\frac{-t}{\tau_{B-S}}\right)}\right) \quad (4.19)$$

The role of the parameters are summarized in table 4.3.

## 4 Concept

$\vartheta_{BAC}$	threshold for the calcium spike (BAC mechanism)
$\vartheta_S$	threshold for the sodium spike
$\tilde{t}$	time of last BAC threshold crossing
$\eta_{BAC}$	form of the plateau voltage applied to the soma through BAC mechanism, should lead to a bursting behaviour of about 30ms [Larkum et al., 2004]
$\eta_S(t - \hat{t})$	form of the $Na^+$ spike and after-spiking potential ([Benuskova, 2003] for examples)
$\alpha_{Norm}$	normalization factor for stochastic threshold
$\tau$	time constant for reset of membrane potential after spike, 1-10ms [Benuskova, 2003]
$\Delta_{dead}$	deadtime

Table 4.3: Variables used in the somatic compartment representation

### Basal Dendritic Compartment (B)

The basal dendritic compartment is the second input integration site of the pyramidal neuron model. As theoretical and experimental data suggest, input data arriving at the apical dendritic tree, will mostly consist of feedback (or top-down) information, while input arriving at dendrites proximal to the soma, most of the basal dendritic tree will deliver feedforward (or sensory) information (for theoretical background see section 3.1.4).

The main function of the basal compartment is the integration of the excitatory and inhibitory postsynaptic potentials.

$$u_B(t) = u_{rest} + \sum_b w_b \sum_f \epsilon_B(t - t_b^f) \quad (4.20)$$

## 4 Concept

The resulting membrane potential of the basal dendritic compartment  $u_B$  is then forward propagated into the soma to contribute to the spiking mechanism.

The role of the parameters are summarized in table 4.4.

$b$	presynaptic neurons connected to the basal compartment
$\epsilon_B(t - t_b^f)$	time course of the response to an incoming spike f

Table 4.4: Variables used in the basal dendritic compartment representation

## 4.2 Simulation Concept

### 4.2.1 Simulation Objectives

The first two simulations are performed to tune the parameters of the pyramidal neuron model to reproduce experimental results. Following the work of [Larkum, 2013] and [Richard Naud and Gerstner, 2013] we modelled the BAC firing mechanism and neuron compartments, which is briefly reviewed here.

Larkum coined the term of the BAC firing mechanism first, describing the effects of active dendrites, propagation and a secondary spike initiation zone in one term. These effects conform with the latest insights in pyramidal neuron biology (see chapter 3) and should also be proven in the simulation. Furthermore, the latest paper by Larkum et al. focuses on the advanced computational abilities of pyramidal neurons by combining two information streams. The ability of a single neuron to perform complex operations like coincidence detection is proposed as one of the main factors determining the advanced capabilities of the cerebral cortex [Larkum, 2013]. In reference to these theoretical assumptions the effects of coincidence detection and dual information stream processing will be also addressed in the simulation (see section 5.4.1).

Naud et al. used a similar two-compartmental model to reproduce the spiking and bursting behaviour of biological pyramidal neurons. The paper provides simulation results about the dependencies between spike and burst occurrences and the respective current levels. These results will be used to tune the parameters of the proprietary pyramidal model (see section 5.4.2)

The third simulation will focus on demonstrating the information processing abilities of the pyramidal neuron model. Two neurons will therefore be connected in series. In addition each neuron will receive a sinusoidal distributed current input overlaid with a spiking poisson input. The network is then manually tuned to perform a filter and coincidence detection

## 4 Concept

operation on the input streams, creating a bursting pattern whenever the input signals are correlated and spikes whenever one of the input signals is active (section 5.4.3).

The forth simulation focusses on the implementation of an abstract parameter learning algorithm. It will be further described in the subsequent section 4.2.2.

In the last simulation a learning algorithm will be implemented which focuses on the adaptation of synaptic weights based on the calcium spiking mechanism (see section 5.4.4).

### 4.2.2 Parameter Learning Algorithm

This simulation will implement an abstract parameter learning algorithm. For this reason the pyramidal neuron is reformulated into a hidden markov model (HMM) representation, which allows the description of hidden states and observables.

A HMM will be necessary as only a few of the variables, such as the somatic membrane potential and spike count, are made observable. The expectation maximization algorithm and its respective version for HMMs, the Baum-Welch algorithm, is proposed as the main parameter learning technique.

The parameter extraction process is shown on the example of the spiking threshold ( $\vartheta$ ). For this reason the somatic membrane potential and the respective output spikes were recorded during a simulation. These values were used to build the state transition matrix. With the use of the Baum-Welch algorithm the spike probability matrix depending on the internal HMM states was inferred. Through adaptation of the pyramidal neuron equations the spiking threshold could then be extracted by using the state at the maximum of the spike probability matrix.

### HMM Translation

Figure 4.2 shows the simulation concept. It outlines the representation of the neuron model as an hidden markov model [Bengio and Frasconi, 1995]. The somatic membrane potential  $u_S$  determines the hidden state  $Y_t$  of the HMM. The spiking output of the neuron serves as observation variable  $X_t$ . The transition probabilities between the states and from each state to the possible observation values are calculated using the Baum-Welch algorithm.

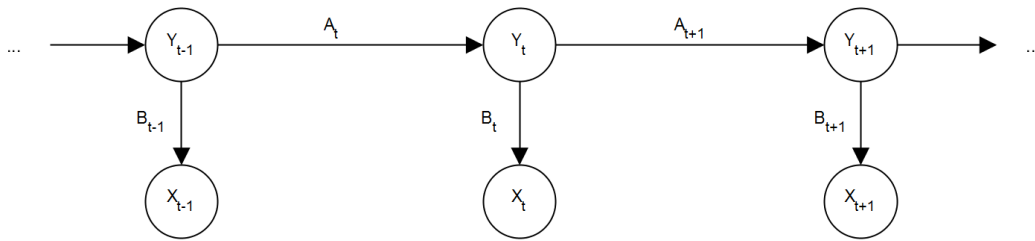


Figure 4.2: HMM Simulation model. The figure shows the Bayesian network HMM representation.  $X_t$  are the observed variables of the model, in this case the spike output of the neuron is used.  $Y_t$  is the hidden state at time  $t$ . The possible voltage levels of the somatic membrane potential are chosen as states of the model. The formulas for the transition probabilities between the states ( $A_t$ ) and the probabilities of a certain state given an observation ( $B_t$ ) are derived from the pyramidal neuron model description in this chapter.

The following equations deal with the translation of the pyramidal neuron model into the hidden markov model. For reasons of simplicity the refractory period after each spike is omitted.

$Y$	hidden states
$X$	output variables
$\theta$	parameters

$$Y = \{u_S\} \quad (4.21)$$

## 4 Concept

$$X = \{Spikeoutput\} \quad (4.22)$$

$$\theta = \{w_A, w_B, \vartheta, \vartheta_{BAC}, u_{BAC}, \alpha\} \quad (4.23)$$

The Probability between states ( $A_t$ ) is calculated by taking into account the exponential decay of the somatic membrane potential  $u_S$ . The spiking probability ( $B_t$ ) is calculated using the stochastic threshold and including both input streams and the BAC mechanism.

$$\begin{aligned} A_t &= P(Y_t = j | Y_{t-1} = i) \\ &= P(u_{S,t} = j | u_{S,t-1} = i) \\ &= \delta(u_{S,t-1} \cdot e^{-t/\tau} - j) \\ &= \delta(i \cdot e^{-t/\tau} - j) \end{aligned} \quad (4.24)$$

Equation 4.24 shows the probability matrix  $A_t$  in between the states  $i$  and  $j$ . The states describe a voltage level of the discretized somatic membrane potential  $u_S$ .

$$\begin{aligned} B_t &= P(X_t = x_t | Y_t = j, \theta) \\ &= P(X_t = Spike/NoSpike | u_{S,t} = j, u_{A,t}, u_{B,t}, \eta_{BAC,t}) \\ &= \exp((u_{S,t} - \vartheta) \cdot \alpha) \cdot ref_{BAC,t} \end{aligned} \quad (4.25)$$

The variable  $\pi_i$  describes the prior probability to the network states  $Y_i$ . In this case the resting potential of the neuron is used as a prior probability, resulting in a delta distribution.

$$\begin{aligned} \pi_i &= P(Y_1 = i) \\ &= \delta(u_{S,t=1} - i) \end{aligned} \quad (4.26)$$

## 4 Concept

The following equations (4.27 - 4.35) show the derivation of the final formulas for  $A_t$  and  $B_t$  as can be viewed in equations 4.36 and 4.37.

$$u_{S,t} = u_{A,t}^{FP} + u_{B,t}^{FP} + BAC + u_{S,t-1} \cdot e^{-t/\tau} \quad (4.27)$$

$$u_{A,t}^{FP} = u_{A,t-1} \cdot \gamma_{A-S}(t) \quad (4.28)$$

$$u_{A,t} = \sum_a w_a \sum_f \epsilon_A(t - t_a^f) + u_{A,t-1} \cdot e^{-t/\tau} + u_{S,t}^{BP} \quad (4.29)$$

$$u_{S,t}^{BP} = u_{S,t-1} \cdot \gamma_{S-A}(t) \quad (4.30)$$

$$u_{B,t}^{FP} = u_{B,t-1} \cdot \gamma_{B-S}(t) \quad (4.31)$$

$$u_{B,t} = \sum_b w_b \sum_f \epsilon_B(t - t_b^f) + u_{B,t-1} \cdot e^{-t/\tau} \quad (4.32)$$

The BAC mechanism is represented as a plateau potential with a fixed burst time (with time constant  $\tau_{BURST}$ ) and a refractory period (with time constant  $\tau_{refr}$ ) following. These times are independent from the spiking time and refractory period following a single spike.

Whenever the voltage in the apical compartment  $u_A$  rises above the BAC threshold  $\vartheta_{BAC}$ , the variable  $\eta_{BAC}$  becomes positive. Afterwards, it decays slowly back to zero via an exponential decay defined by  $\tau_{BURST}$ . During this time, the heaviside step function  $H()$  is applied to  $\eta_{BAC}$  and multiplied with  $u_{BAC}$ , resulting in the intermediate variable  $BAC$  representing the plateau potential which is directly applied to the somatic membrane potential.

$$BAC = H(\eta_{BAC,t}) \cdot u_{BAC} \quad (4.33)$$

## 4 Concept

$$\eta_{BAC,t} = \eta_{BAC,t-1} \cdot e^{-t/\tau_{BURST}} + u_{A,t-1} - \vartheta_{BAC} \quad (4.34)$$

The refractory period after a bursting period is calculated using equation 4.35. The term  $(1 - H(\eta_{BAC,t} \cdot e^{-t/\tau_{BURST}}))$  is the inverse of equation 4.33. It is 1 except during the plateau potential period, where it takes the value zero.

$(e^{-t/(\tau_{BURST} + \tau_{refr})})$  on the other hand is only positive during the plateau potential period and the refractory period afterwards. By multiplying the two terms, only the refractory period remains. After that, the heaviside step function is again applied to the term and subtracted by 1, which leads to a term which is only positive outside of the refractory period after the bursting. By multiplication of this term  $ref_{BAC}$  to the spiking probability the refractory period is applied.

$$ref_{BAC,t} = 1 - H((\eta_{BAC,t} \cdot e^{-t/(\tau_{BURST} + \tau_{refr})}) \cdot (1 - H(\eta_{BAC,t} \cdot e^{-t/\tau_{BURST}}))) \quad (4.35)$$

By combining the equations above, the final results for  $A_t$  and  $B_t$  are obtained representing figure 4.2:

$$\begin{aligned} A_t &= P(Y_t = j | Y_{t-1} = i) \\ &= P(u_{S,t} = j | u_{S,t-1} = i) \\ &= \delta(u_{S,t-1} \cdot e^{-t/\tau} - j) \\ &= \delta(i \cdot e^{-t/\tau} - j) \end{aligned} \quad (4.36)$$

#### 4 Concept

$$\begin{aligned}
B_t &= P(X_t = x_t | Y_t = j, \theta) \\
&= P(X_t = Spike/NoSpike | u_{S,t} = j, u_{A,t}, u_{B,t}, \eta_{BAC,t}) \\
&= \exp\left(\left(\sum_a w_a \sum_f \epsilon_A(t - t_a^f) + u_{A,t-1} \cdot e^{-t/\tau} + u_{S,t-1} \cdot \gamma_{S-A}(t)\right) \cdot \gamma_{A-S}(t) \right. \\
&\quad \left. + \left(\sum_b w_b \sum_f \epsilon_B(t - t_b^f) + u_{B,t-1} \cdot e^{-t/\tau}\right) \cdot \gamma_{B-S}(t) \right. \\
&\quad \left. + H(\eta_{BAC,t-1} \cdot e^{-t/\tau_{BURST}} + u_{A,t-1} - \vartheta_{BAC}) \cdot u_{BAC} \right. \\
&\quad \left. + u_{S,t-1} \cdot e^{-t/\tau} - \vartheta\right) \cdot \alpha \\
&\quad \cdot \left(1 - H(\eta_{BAC,t} \cdot e^{-t/(\tau_{BURST} + \tau_{refr})}) \cdot \left(1 - H(\eta_{BAC,t} \cdot e^{-t/\tau_{BURST}})\right)\right)
\end{aligned} \tag{4.37}$$

Through mathematical rearrangement the HMM representation can be changed, leading to the formula 4.38 (only changed formulas are printed):

$$\begin{aligned}
B_t &= \exp\left(\left(\sum_a w_a \sum_f \epsilon_A(t - t_a^f) + u_{A,t-1} \cdot e^{-t/\tau}\right) \cdot \gamma_{A-S}(t) \right. \\
&\quad \left. + \left(\sum_b w_b \sum_f \epsilon_B(t - t_b^f) + u_{B,t-1} \cdot e^{-t/\tau}\right) \cdot \gamma_{B-S}(t) \right. \\
&\quad \left. + H(\eta_{BAC,t-1} \cdot e^{-t/\tau_{BURST}} + u_{A,t-1} + u_{S,t-1} \cdot \gamma_{S-A}(t) - \vartheta_{BAC}) \cdot u_{BAC} \right. \\
&\quad \left. + u_{S,t-1} \cdot (e^{-t/\tau} + \gamma_{S-A}(t) \cdot \gamma_{A-S}(t)) - \vartheta\right) \cdot \alpha \\
&\quad \cdot \left(1 - H(\eta_{BAC,t} \cdot e^{-t/(\tau_{BURST} + \tau_{refr})}) \cdot \left(1 - H(\eta_{BAC,t} \cdot e^{-t/\tau_{BURST}})\right)\right)
\end{aligned} \tag{4.38}$$

## 4 Concept

### Parameter estimation

**Threshold** After the translation of the model into a HMM representation in section 4.2.2 the Baum-Welch algorithm is used to get the estimated probability distributions.

Therefore the somatic membrane potential  $u_S$  is discretized linearly into  $V$  steps ranging from its minimum value at the resting membrane potential to the maximum above threshold level. The prior probability  $\pi_i$  of each state can be set using a delta distribution, as the probability is only 1 for the resting potential.

The transition probability matrix between the states  $i$  and  $j$   $A_{i,j}$  (see figure 4.4) is determined by the time course of the somatic membrane potential.

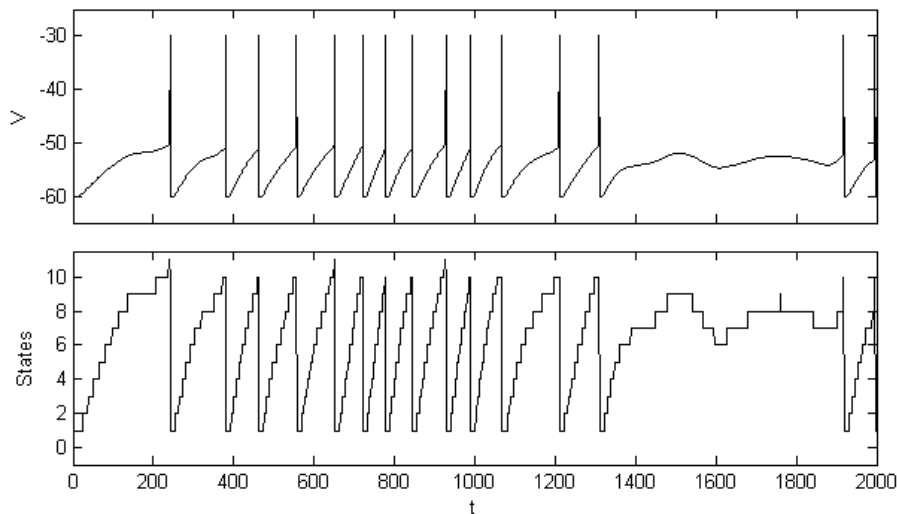


Figure 4.3: Discretized somatic membrane potential. The upper plot shows the somatic membrane potential  $u_S$  measured during the simulation. The lower plot shows the discretized somatic membrane potential. The voltage was divided into ten discrete steps, which serve as the internal state of the HMM.

## 4 Concept

0.90	0.10	0	0	0	0	0	0	0	0	0
0	0.45	0.55	0	0	0	0	0	0	0	0
0	0	0.38	0.62	0	0	0	0	0	0	0
0	0	0	0.37	0.63	0	0	0	0	0	0
0	0	0	0	0.42	0.58	0	0	0	0	0
0	0	0	0	0	0.41	0.59	0	0	0	0
0	0	0	0	0	0	0.42	0.58	0	0	0
0	0	0	0	0	0	0	0.44	0.56	0	0
0	0	0	0	0	0	0	0	0.44	0.56	0
0.36	0	0	0	0	0	0	0	0	0.48	0.17
0	0	0	0	0	0	0	0	0	0.96	0.04

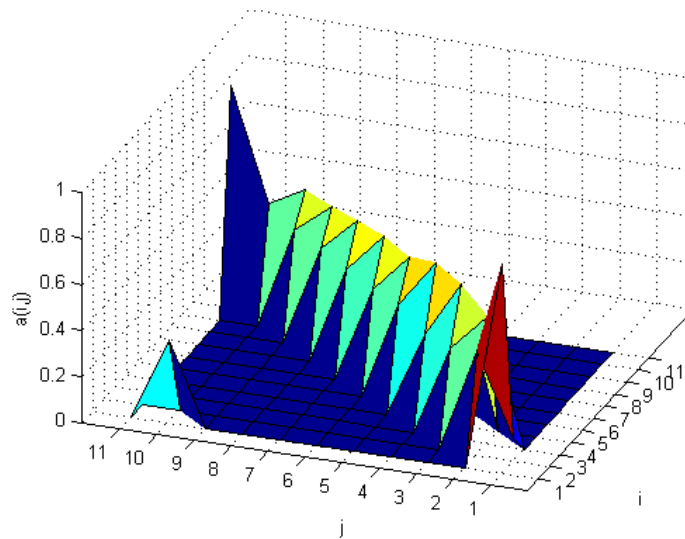


Figure 4.4: State transition matrix A. The plot shows the transition probabilities between any two states  $i$  and  $j$ . It can already be observed that the states are progressive with state  $i$  leading to state  $i + 1$  until the threshold is reached.

After setting the initial probabilities  $\pi$  and  $A_t$  the probability matrix  $B_t$  is randomly initialized and trained using the Baum-Welch algorithm (see figure 4.5).

## 4 Concept

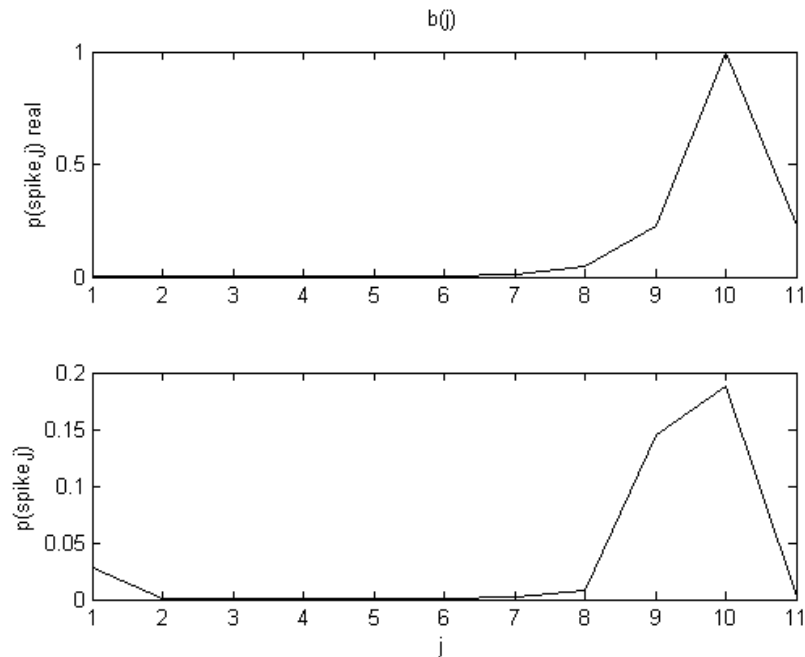


Figure 4.5: Spike probability matrix  $B$ . The upper plot shows the real distribution of the spiking probability over all states. The highest probability is at state 10 (which equals  $-50mV$ , the threshold level in the simulation). As a stochastic threshold is used, there is also a smaller probability that the neuron spikes before reaching the threshold which was mapped as an exponential decay. The lower plot shows the predicted probability distribution after application of the Baum-Welch algorithm.

With the use of the predicted probability distribution matrix  $B_t$  the threshold value can be extracted.

The theoretical formula for the probability matrix  $B_t$  was already derived in the previous section 4.2.2.

Equation 4.25 is now used to extract a formula for the threshold value.

For this reason the state with the highest spiking probability (state at  $B_{max}$ ) is used. This state value is used to infer about the underlying threshold level. The BAC refractory period can be omitted in this formula as no burst

#### 4 Concept

was detected.

$$\begin{aligned} B_{max} &= \exp((u_S - \vartheta) \cdot \alpha) \\ \frac{B_{max}}{\alpha} &= \exp((u_S - \vartheta)) \\ \log\left(\frac{B_{max}}{\alpha}\right) &= u_S - \vartheta \\ \vartheta &= u_S - \log\left(\frac{B_{max}}{\alpha}\right) \end{aligned} \tag{4.39}$$

# 5 Implementation

This chapter describes how the proprietary NEST implementation of the pyramidal neuron can be used. The parameters which are adjustable are listed, as well as their respective default values (section 5.1 and 5.3). Further some mathematical translations, which were necessary to comply with the NEST environment, are shown.

The second part of this chapter shows the carried out simulations in order to compare the implemented model with experimental data and show some application examples of the model as a gateway function and for learning (section 5.4).

## 5.1 General description

The NEST implementation currently holds four compartments (Apical, Oblique, Somatic and Basal). Every compartment, except the somatic one, is able to receive excitatory and inhibitory synaptic inputs.

The synaptic inputs can be adjusted in weights when connecting them to the pyramidal neuron model. Furthermore, the time constant for excitatory and inhibitory inputs can be adjusted. The resulting input spike can be read out with or without the connected weight.

Moreover, all compartments are able to receive a static current input and a changing current over time.

The spike and BAC mechanism threshold can be adjusted as well as the resting potentials of all four compartments. The duration of the plateau

## 5 Implementation

potential and the refractory period after a spike and after the BAC mechanism can be further changed. Stochasticity is enabled for both single spike events and BAC threshold crossings. The stochasticity value can be adjusted between 0.0 (stochastic firing independent of threshold, leading to constant spiking) and 100.0 (no stochasticity, spikes are emitted exactly at threshold crossing).

In addition the low pass values between the compartments can be changed. In this revision only three values (Apical to Soma, Basal to Soma, Soma to Apical) are used.

### 5.2 Mathematical translation

In accordance with the discrete time steps used in the NEST simulation environment, a discrete integration of some mathematical formulas has to be performed. This was done using the techniques provided in [Rotter and Diesmann, 1999] [Hirsch et al., 1974].

#### 5.2.1 EPSP Kernel

The EPSP time course, represented by  $\epsilon_x$  with  $x$  naming the corresponding compartment, has to be translated.

The conversion is shown here using the example of the apical dendritic compartment, therefore  $\epsilon_a$ . The time-continuous representation of the kernel is as follows:

$$\epsilon_a(t) = t \cdot e^{\left(\frac{-t}{\tau_{Rise}}\right)} \quad (5.1)$$

Epsilon follows the Alpha Function (See upper left part in figure 5.1). For reasons of readability  $1/\tau_{Rise}$  is substituted with the symbol  $a$  in the follow-

## 5 Implementation

ing equations.

$$\epsilon_a(t) = t \cdot e^{-t \cdot a} \quad (5.2)$$

This can be rewritten as:

$$\epsilon_a''(t) + (2a)\epsilon_a'(t) + a^2\epsilon_a(t) = 0 \quad (5.3)$$

In order to solve this 2<sup>nd</sup> order differential equation it is divided into two first order differential equations:

$$\begin{aligned} y_1 &= a\epsilon + \epsilon' \\ y_2 &= \epsilon \end{aligned} \quad (5.4)$$

The derivations are therefore as follows:

$$\begin{aligned} y_1' &= -a \cdot y_1 \\ y_2' &= y_1 - a \cdot y_2 \end{aligned} \quad (5.5)$$

The new existing system is now rewritten in Matrix style:

$$y' = A \cdot y + b \cdot x \quad (5.6)$$

$$\begin{bmatrix} y_1' \\ y_2' \end{bmatrix} = A \cdot \begin{bmatrix} y_1 \\ y_2 \end{bmatrix} + \begin{bmatrix} 0 \\ 0 \end{bmatrix} \quad (5.7)$$

$$\begin{bmatrix} y_1' \\ y_2' \end{bmatrix} = \begin{bmatrix} -a & 0 \\ 1 & -a \end{bmatrix} \cdot \begin{bmatrix} a\epsilon + \epsilon' \\ \epsilon \end{bmatrix} \quad (5.8)$$

The time discrete version of  $y$  can afterwards be calculated using the formula  $y_{k+1} = e^{A\Delta} \cdot y_k + x_{k+1}$  according to [Rotter and Diesmann, 1999].

$$e^{A\Delta} = \begin{bmatrix} e^{-\Delta a} & 0 \\ \Delta \cdot e^{-\Delta a} & e^{-\Delta a} \end{bmatrix} \text{ in reference to [Hirsch et al., 1974]} \quad (5.9)$$

## 5 Implementation

$y_1$  and  $y_2$  were afterwards added up and create the Alpha shaped postsynaptic potential when added to the membrane potential.

The Alpha function was applied to all possible excitatory and inhibitory synaptic inputs of the model. The shape can be varied by changing the parameter  $\tau_{Rise}$  for the respecting compartment.

## 5 Implementation

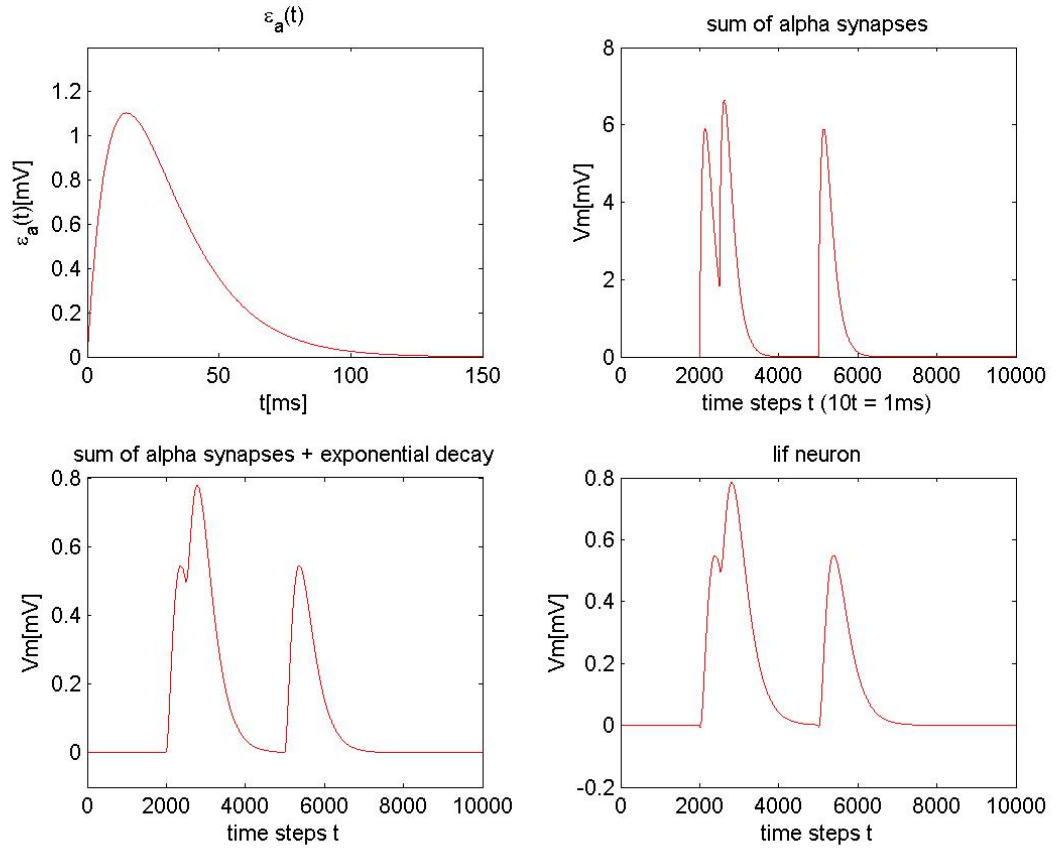


Figure 5.1: Alpha synapse function and membrane potential. The upper left subplot shows the alpha function which is applied to the synaptic input and creates the EPSP. The upper right subplot shows the application of the alpha function to three input spikes. The lower left subplot shows the EPSPs of the three input spikes with an additional exponential decay. Finally the lower right figure shows the time course of the membrane potential for three input spikes when applied to a leaky integrate-and-fire neuron in NEST. When comparing the lower two subplots it can be seen that a synaptic alpha function in addition to an exponential decay can obtain a similar behaviour with a much easier description.

## 5 Implementation

Lowpass:

$$u_S^{BP}(t) = u_S \cdot \left(1 - e^{\left(\frac{-t}{\tau_{S-A}}\right)}\right) \quad (5.10)$$

$$u_A(t) = u_{rest} + \sum_a w_a \epsilon_a(t - \hat{t}) + u_S^{BP}(t) \quad (5.11)$$

### 5.3 NEST Simulation Parameters

The following tables list the parameters that can be read out or set during simulation.

The values filled in have been adjusted in order to fit to the biological basis of the Larkum papers [Larkum et al., 2004][Larkum et al., 1999]

#### 5.3.1 General Parameters

type	name	value
parameters	parameter name	standard value
resting potential after spike	V_reset	-60.0
spike threshold	V_th	-55.0
refractory period after spike	t_ref	2.0
plateau potential activated due to BAC mechanism	V_bac	-54.0
bac mechanism threshold	V_th_bac	-30.0
bac mechanism refractory period	t_ref_bac	0.1
time constant for plateau potential	t_spike_bac	5.0
stochastic threshold factor	alpha	2.5
stochastic threshold factor for BAC mechanism	alpha_bac	unused

Table 5.1: General simulation parameters

## 5 Implementation

### 5.3.2 Apical Compartment

type	name	value
inputs	receptor name	preferred weight
excitatory synaptic inhibitory synaptic current	apical_exc apical_inh apical_current	1800.0 unknown -
parameters	parameter name	standard value
membrane capacitance	C_m	250.0
membrane time constant	tau_m	10.0
excitatory synaptic rise time	tau_syn_ex	2.0
inhibitory synaptic rise time	tau_syn_in	2.0
static current	I_e	0.0
minimum potential	V_min	$-\infty$
resting potential	E_L	-70
low pass time constant to Apical compartment	LPA	0.0
low pass time constant to Oblique compartment	LPO	0.0
low pass time constant to Somatic compartment	LPS	150.0
low pass time constant to Basal compartment	LPB	0.0
observable values	record name	
membrane potential	V_m.A	
excitatory input spikes	spikes_ex.A	
inhibitory input spikes	spikes_in.A	
excitatory input spikes with weight	weighted_spikes_ex.A	
inhibitory input spikes with weight	weighted_spikes_in.A	

Table 5.2: Simulation parameters for apical dendritic compartment

## 5 Implementation

### 5.3.3 Oblique Compartment

type	name	value
inputs	receptor name	preferred weight
excitatory synaptic inhibitory synaptic current	oblique_exc oblique_inh oblique_current	unknown unknown -
parameters	parameter name	standard value
membrane capacitance	C_m	250.0
membrane time constant	tau_m	10.0
excitatory synaptic rise time	tau_syn_ex	2.0
inhibitory synaptic rise time	tau_syn_in	2.0
static current	I_e	0.0
minimum potential	V_min	$-\infty$
resting potential	E_L	-70
low pass time constant to Apical compartment	LPA	0.0
low pass time constant to Oblique compartment	LPO	0.0
low pass time constant to Somatic compartment	LPS	0.0
low pass time constant to Basal compartment	LPB	0.0
observable values	record name	
membrane potential	V_m.O	
excitatory input spikes	spikes_ex.O	
inhibitory input spikes	spikes_in.O	
excitatory input spikes with weight	weighted_spikes_ex.O	
inhibitory input spikes with weight	weighted_spikes_in.O	

Table 5.3: Simulation parameters for oblique dendritic compartment

## 5 Implementation

### 5.3.4 Somatic Compartment

type	name	value
inputs	receptor name	preferred weight
current	soma_current	-
outputs	receptor name	preferred weight
spike event	-	-
parameters	parameter name	standard value
membrane capacitance	C_m	250.0
membrane time constant	tau_m	10.0
static current	I_e	0.0
minimum potential	V_min	$-\infty$
resting potential	E_L	-70
low pass time constant to Apical compartment	LP.A	3.0
low pass time constant to Oblique compartment	LP.O	0.0
low pass time constant to Somatic compartment	LP.S	0.0
low pass time constant to Basal compartment	LP.B	0.0
observable values	record name	
membrane potential	V_m.S	

Table 5.4: Simulation parameters for somatic compartment

## 5 Implementation

### 5.3.5 Basal Compartment

type	name	value
inputs	receptor name	preferred weight
excitatory synaptic inhibitory synaptic current	basal_exc basal_inh basal_current	40.0 unknown -
parameters	parameter name	standard value
membrane capacitance	C_m	250.0
membrane time constant	tau_m	10.0
excitatory synaptic rise time	tau_syn_ex	2.0
inhibitory synaptic rise time	tau_syn_in	2.0
static current	I_e	0.0
minimum potential	V_min	$-\infty$
resting potential	E_L	-70
low pass time constant to Apical compartment	LPA	0.0
low pass time constant to Oblique compartment	LPO	0.0
low pass time constant to Somatic compartment	LPS	15.0
low pass time constant to Basal compartment	LPB	0.0
observable values	record name	
membrane potential	V_m.B	
excitatory input spikes	spikes_ex.B	
inhibitory input spikes	spikes_in.B	
excitatory input spikes with weight	weighted_spikes_ex.B	
inhibitory input spikes with weight	weighted_spikes_in.B	

Table 5.5: Simulation parameters for basal dendritic compartment

### 5.4 Simulation Results

#### 5.4.1 Comparison to Larkum Paper

The focus of this simulation was to compare the proprietary layer 5 pyramid model with the experimental results obtained in [Larkum, 2013]. It could be shown, that with correct parameter tuning, the pyramidal neuron model behaves similar to the biological records obtained by Larkum et al.

In the first figure 5.2 the experimental setup can be observed. Two independent input signals were applied on two locations of a layer 5 pyramidal neuron. A small current pulse (blue) was applied to the basal dendrite, while a current spike (red) was applied to the apical dendrite. The experiment showed that the basal current was able to trigger single output spikes, but only a coincident application of the apical and basal current triggered the internal calcium spike mechanism which resulted in a burst of three action potentials.

These experimental findings were replicated using the proprietary model. The results can be observed in figures 5.3-5.5. The figures show the membrane potentials in the upper part of the figure and the spike and current events applied to the neuron in the lower part.

## 5 Implementation

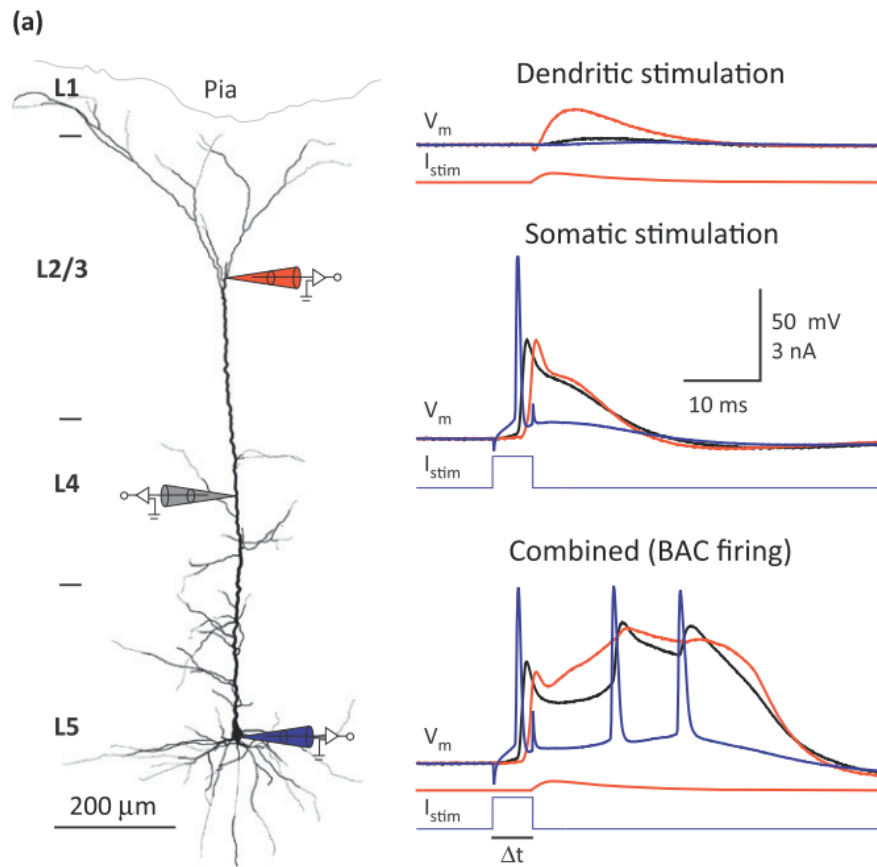


Figure 5.2: Figure taken from [Larkum, 2013] for reasons of comparison. Larkum showed the effects of a single dendritic spike input (red curve,  $I_{stim}$ ) and a basal dendritic current pulse (blue curve,  $I_{stim}$ ). The figure shows that a single apical spike input does not trigger a spike, but propagates into the somatic compartment. A single basal input current on the other hand is able to trigger a single somatic output spike, and it propagates into the soma as well as into the apical dendritic tree. The last plot on the right shows the influence of a combined apical spike and basal current input. The combined input triggers a dendritic calcium spike which is represented as a long apical plateau potential.

## 5 Implementation

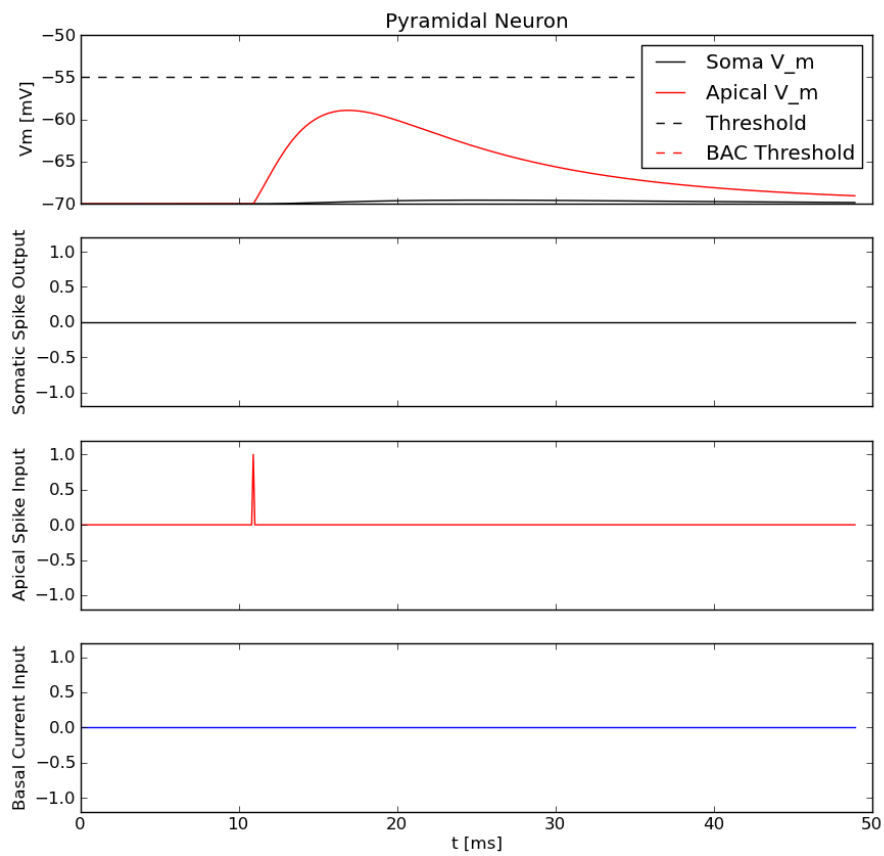


Figure 5.3: Simulation of an apical input spike in reference to Figure 5.2. The figure shows the development of the somatic and apical membrane potential (first plot) as well as the somatic spike output (second plot), the apical spike input and the basal dendritic current input (third and fourth plot). The first plot shows that the apical dendritic spike input forces a membrane potential uprising in the form of an alpha synapse. This potential is propagated to the somatic compartment, which also shows a rising voltage potential. However no output spike is produced as the somatic membrane potential is always below threshold (black dotted line)

## 5 Implementation

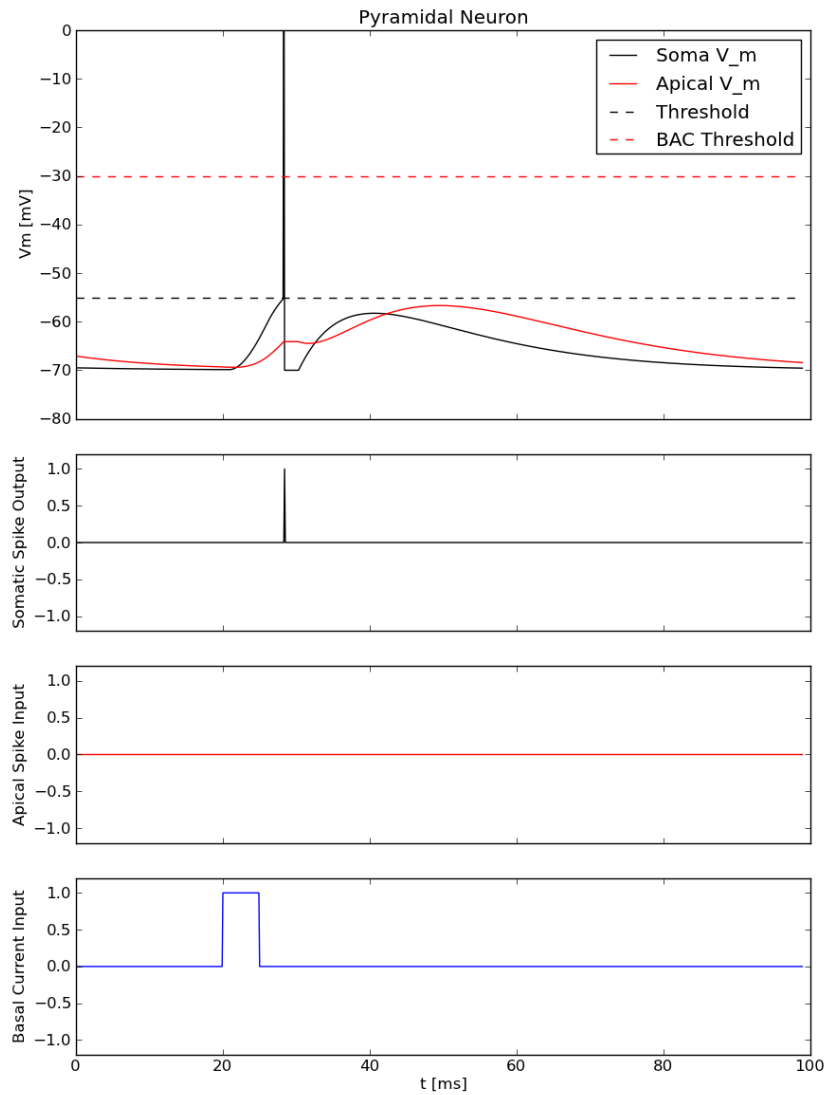


Figure 5.4: Simulation of a basal input current in reference to Figure 5.2. The forth plot on the bottom shows the input current applied to the basal dendritic compartment. This leads to a rising somatic membrane potential (first plot, black curve) until the spiking threshold (black dashed line) is reached and a spike is omitted. The first plot also shows that the basal and somatic membrane potential propagate into the apical dendritic compartment, leading to a small rise of the apical membrane potential as well (red curve)

## 5 Implementation

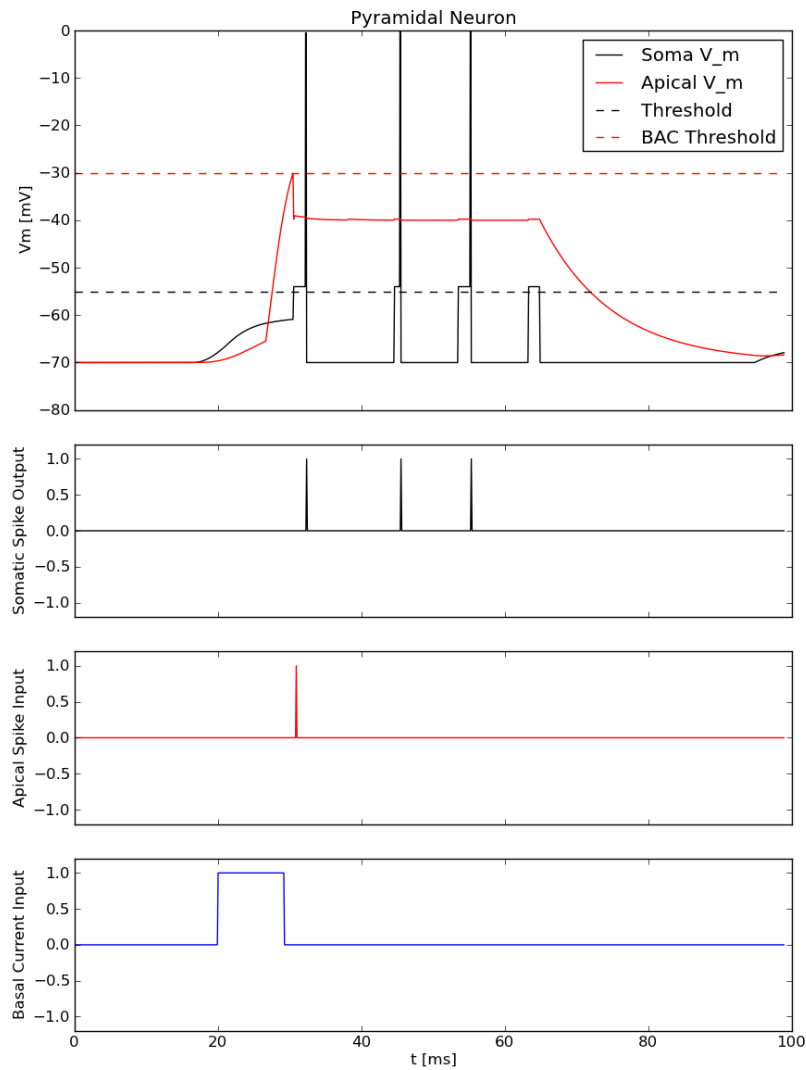


Figure 5.5: Simulation of a combined apical spike/basal current input in reference to Figure 5.2. The figure shows the influence of a combined input of a current applied to the basal compartment (forth plot) and a spike input applied to the apical dendritic compartment (third plot). As can be seen in the first plot, the combined input leads to a rise in the somatic membrane potential (black curve). Additionally the basal membrane potential is propagated into the apical compartment, forcing a rise of the apical membrane potential (red curve). This rise of the apical potential in combination with the apical spike input leads to a threshold crossing for a dendritic Calcium spike (red dashed line). The calcium spike is represented by a long plateau potential which gets propagated into the somatic compartment and forces a burst (here: three) of APs.

## 5 Implementation

As in the Larkum paper, a single dendritic stimulation (as simulated at 10ms using excitatory synaptic input) only minor changed the somatic potential. A somatic current injection (here simulated with current input to the somatic compartment at 110ms) caused a single spike to occur and be also backpropagated to the apical compartment causing a rise in the potential.

Finally, the combined input (current injected in the soma followed by a small dendritic input at 220ms) induced the BAC firing mechanism and caused a short burst of action potentials in the soma. The duration of the plateau potential was adjusted in order to conform with the number of spikes observed in the biological cell.

### 5.4.2 Comparison to Naud Paper

The objective of this simulation was to compare the proprietary layer 5 pyramidal neuron to the experimental results from [Richard Naud and Gerstner, 2013].

Naud et al. recorded the mean currents applied to the apical dendritic tree and the soma of a pyramidal neuron. The currents were then plotted around the detected output spikes and output bursts of the neuron, which are shown in figure 5.6.

The experiments especially focussed on the current distribution exactly at the spike and burst trigger time. They showed that the somatic current is always higher around a triggered output spike, while the apical current is higher around a triggered burst.

These results were compared with the proprietary model. Figure 5.7 shows the average current applied to the pyramidal neuron 20ms before and after a spike (upper subfigure) and after a burst (lower subfigure). A burst was detected using the definition from [Larkum et al., 2004]. A burst was defined as at least three APs within 20ms and less than three APs in the preceding 20ms.

## 5 Implementation

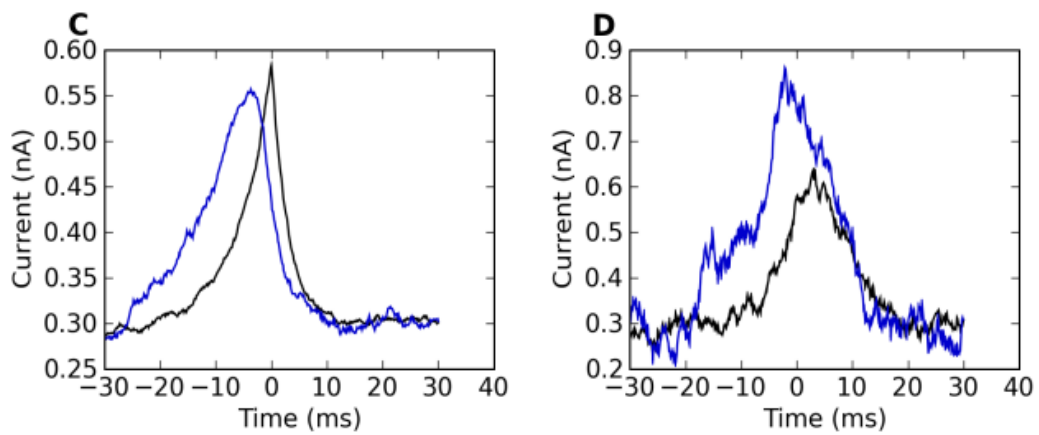


Figure 5.6: Figure taken from [Richard Naud and Gerstner, 2013] for reasons of comparison. Two random input currents were applied to the apical dendrite and the soma. After that the spike and burst events of the neuron were detected and the input currents around all spike and burst events were summed up. The two plots show the input currents around a spike event (plot C, spike is triggered at time  $t = 0$ ) and a burst event (plot D, burst is triggered at time  $t = 0$ ).

## 5 Implementation

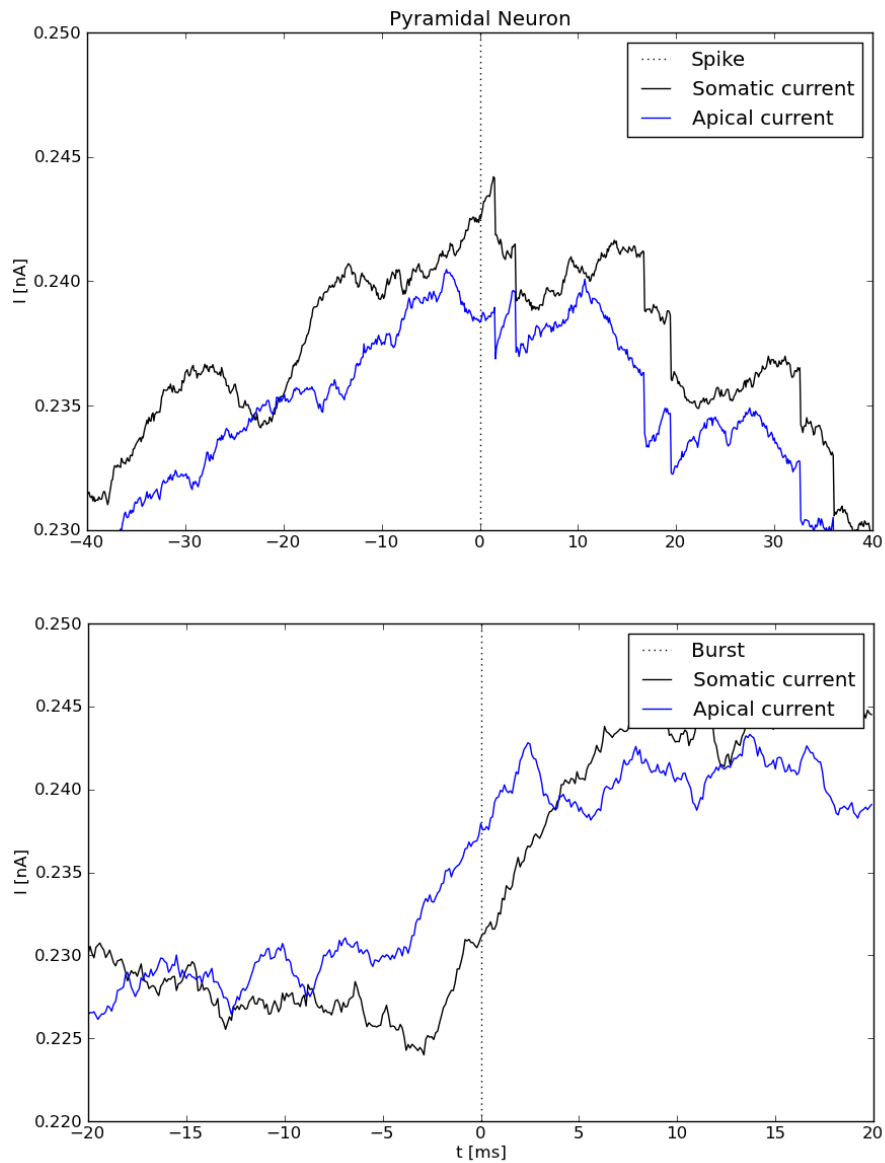


Figure 5.7: Average current around spikes (upper subplot) and bursts (lower subplot) in reference to Figure 5.6. The upper subplot shows the input current applied to the somatic compartment (black curve) and the input current applied to the apical dendritic compartment (blue curve), as measured around all triggered output spikes of the neuron. It shows that the somatic current has got a higher peak around the single spikes, therefore it is determining the spiking behaviour. The lower subplot shows the input currents as measured around all detected output bursts. Here the plot shows that the apical current has got a higher potential around the bursting time, therefore determining the bursting mechanism.

## 5 Implementation

In the simulation a poisson current was applied to both the apical and the basal dendritic compartment. Backward- and forwardpropagation was used as in the experiment before. Compared to figure 5.6 taken from [Richard Naud and Gerstner, 2013], the current values are smaller and the current leading to bursting behaviour is rising after the burst event. This can be explained by the applied plateau potential which was not used in the experiment from [Richard Naud and Gerstner, 2013]. Otherwise the behaviour of the simulations match. For the spiking current the somatic current has got a higher peak, determining the spiking behaviour. Concerning bursts, on the other hand, the apical current is higher.

### 5.4.3 Coincidence Detection via Manual Parameter Tuning

This section describes the simulation results obtained by using two L5 pyramidal neurons in series and tuning the parameters to get a two-fold coincidence detection. The results can be interpreted as a low-level filter mechanism finding abstract object representations by coincidence detection with a given feedback signal and forwarding the resulting objects depending on the current attention level. Figure 5.8 shows the simulation setup. For reasons of simplicity the oblique dendritic compartment is not used in the current model simulations.

## 5 Implementation

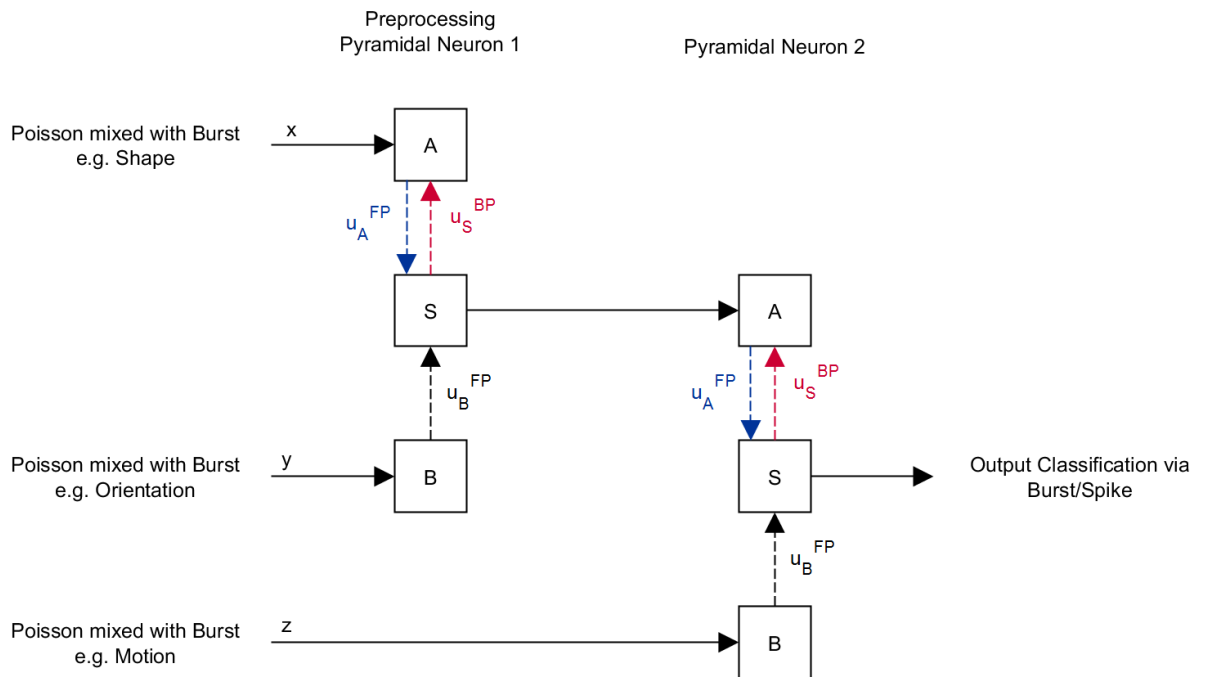


Figure 5.8: Possible connectivity model of two pyramidal neurons. The plot shows the two steps in information processing. First of all the left pyramidal neuron performs a coincidence detection of the input streams  $x$  and  $y$ . The output of the first neuron serves as input for the apical compartment of the second neuron. The second neuron on the right then performs a coincidence detection of the first output and the third input stream  $z$ .

The following figures 5.9 and 5.10 show the possible behaviour of two interconnected pyramidal neurons as displayed in 5.8.

In this case the preprocessing pyramidal neuron performs a sensible coincidence detection between the first two input streams (figure 5.9, red and blue input streams, black output spiking pattern), resulting in bursting behaviour whenever both inputs are correlated.

The post-processing neuron uses the third input stream as a gateway function. Whenever the third input stream (blue signal) shows none to less activity, all signal passing is blocked, otherwise the output stream generated by the preprocessing neuron (red input) is passed on unchanged.

## 5 Implementation

At this time of the simulation only excitatory synaptic inputs are used. By also using also inhibitory synapses in both the apical and the basal compartment, more complex input-output functions can be modelled.

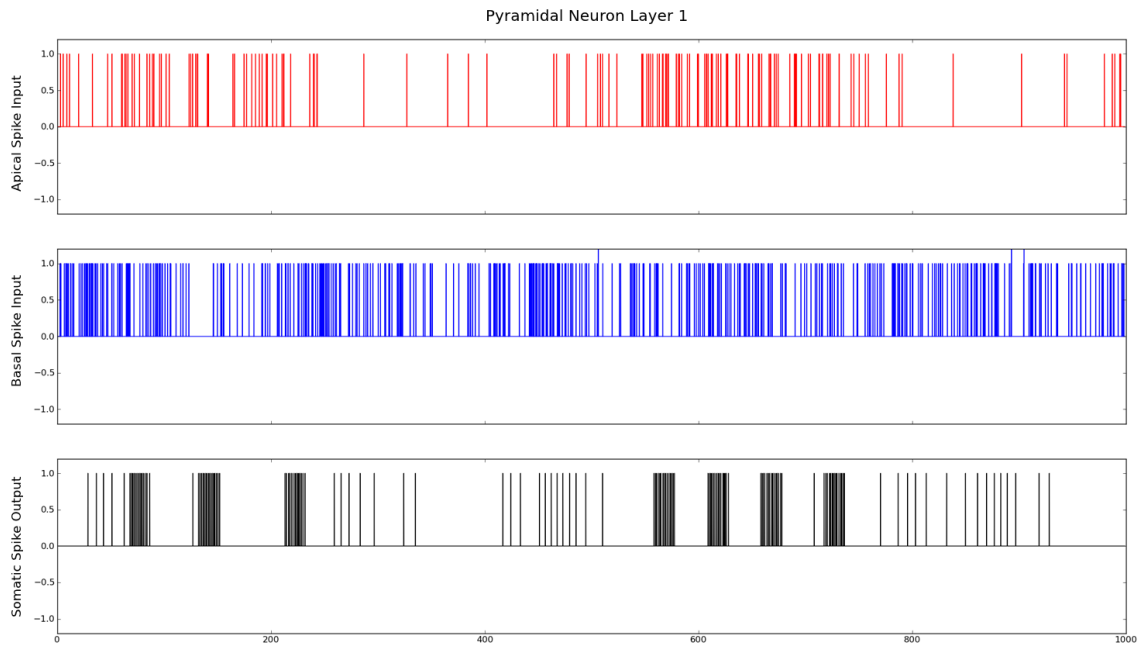


Figure 5.9: Input-Output activity of the pyramidal neuron in layer 1. The figure shows two synaptic input streams. The apical input stream (red) arriving at the distal apical dendritic compartment and the basal input stream (blue) arriving at the basal dendritic compartment of the pyramid. The last plot on the bottom shows the output behaviour of the neuron according to the inputs. It can be observed that the basal input causes the neuron to spike, but only coincident input of both apical and basal spikes triggers the internal calcium spike mechanism and forces an output burst.

## 5 Implementation

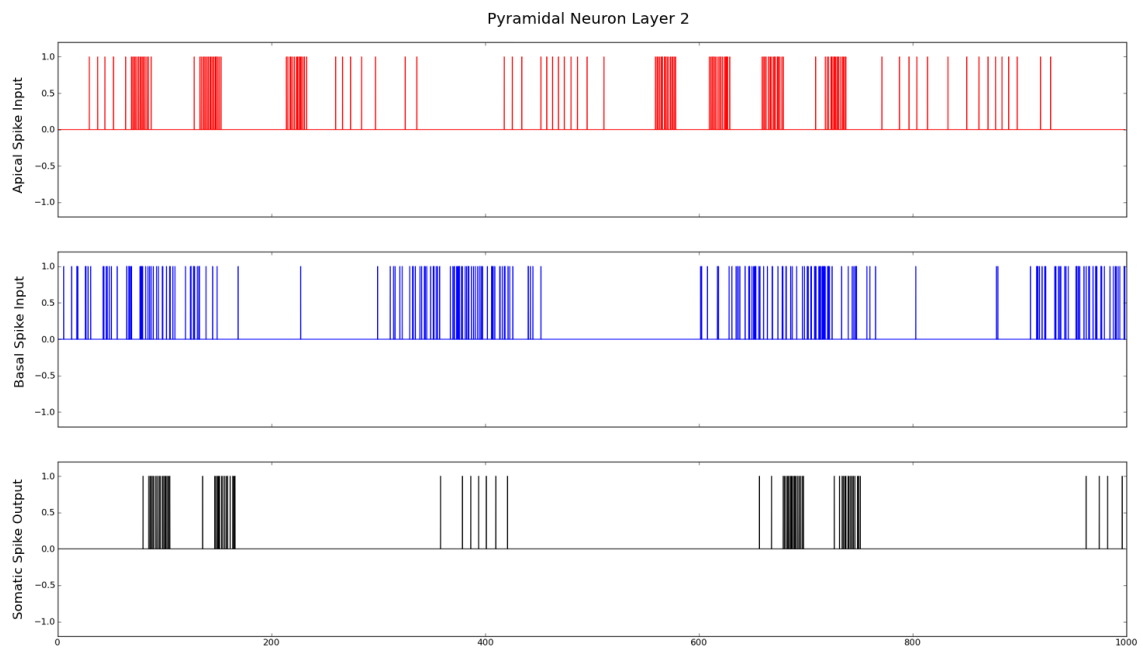


Figure 5.10: Input-Output activity of the pyramidal neuron in layer 2. In this simulation the output of the first pyramidal neuron (see figure 5.9) is used as input to the apical dendritic compartment of the second pyramidal neuron (red). To the basal dendritic compartment a sinusoidal poisson input is applied (blue). Even though bursts are received in the apical compartment, the calcium mechanism is only triggered if minor basal input is applied coincidentally. The second neuron can therefore be viewed as a gateway function, which lets the output of the first neuron through whenever any kind of basal activity is present. This simple mechanism could may be relayed to attention (see chapter 3

### 5.4.4 Learning Algorithm

In this simulation a pyramidal neuron was applied with five apical and five basal input streams. Each input stream attached itself to the pyramidal neuron compartment with an initial synaptic connection weight.

The weights were only altered during an active calcium spike (output burst) of the neuron. During the bursting period the synaptic weights of active inputs were strengthened by a linear factor, while non-active inputs were weakened. After some training time the weights have properly adapted. Only the weights of input synapses which showed coincident activation during the bursts were increased according to their activity.

## 5 Implementation

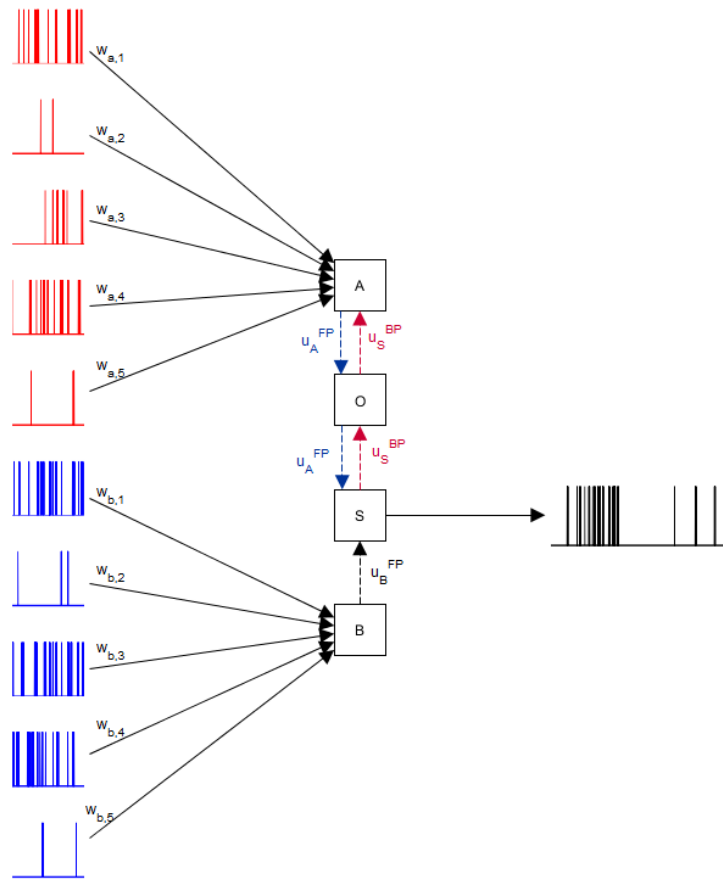


Figure 5.11: Connection model of the pyramidal neuron with five apical and five basal synaptic inputs. The figure shows the setup for the simulation consisting of one pyramidal neuron with five apical synaptic inputs ( $w_{a,1} - w_{a,5}$ ) and five basal synaptic inputs ( $w_{b,1} - w_{b,5}$ ). The pyramidal neuron will trigger bursts whenever two inputs are active at the same time. During the bursting period, the synaptic weights of the inputs active are strengthened, while inactive synapses are weakened.

## 5 Implementation

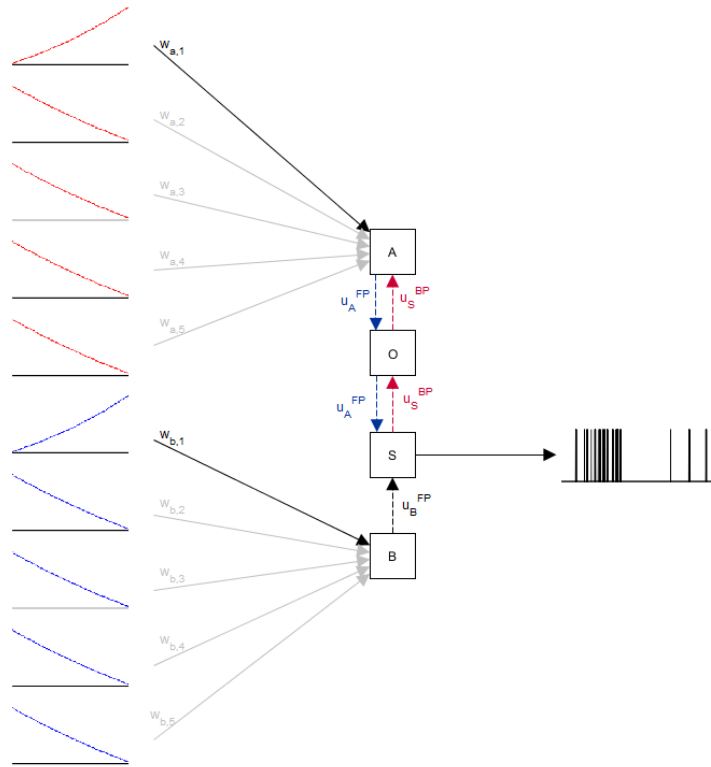


Figure 5.12: Evolution of the synaptic weights during learning. The figure shows the schematic end result of the synaptic weight learning. The plot on the left displays the weight development of the five apical and five basal synaptic weights. It can be observed that the first apical and basal synaptic weight was strengthened, while all other weights were weakened. This was obtained because only the first two synaptic input streams were active at the same time, as can be observed in figure 5.13

The weight update rule was based on the experiment by [Körding and König, 2000]. Körding et al. compared the apical dendritic membrane potential of their neuron model to a threshold. Whenever the apical membrane potential exceeded the threshold a learning event was induced, which allowed synaptic plasticity. During this learning phase the synaptic weights were updated according to their pre-synaptic firing rate.

## 5 Implementation

In this experiment we used a similar algorithm. As the pyramidal neuron model only sends out spike events, the firing rate had to be extracted by averaging over  $T = 100$  time steps with a  $\Delta t$  of  $0.1ms$  (see equation 5.12).

$$rate(t, \dots, t + T) = \frac{\sum_t^{t+T} spike_t}{T} \quad (5.12)$$

Whenever a calcium spike is triggered due to the BAC firing mechanism, an output burst is automatically created. This burst reflects in the output firing rate of the pyramidal neuron.

An output burst was declared whenever the firing rate of the pyramidal neuron exceeded a threshold value (see figures 5.13 to 5.16, the plot on the bottom shows the mean output firing rate of the neuron with the red curve marking burst events. As can be observed the detected bursts match with the internal calcium spike events).

The activation of each synapse during the bursting phase was then calculated by summing over all pre-synaptic spikes  $f$  caused by a single synaptic input  $i$  during the bursts. This value was then averaged over all pre-synaptic spikes during the bursting period of the neuron (see equation 5.13).

$$\alpha(i) = \frac{\sum_f spike_i}{\sum_i \sum_f f spike_i} \quad (5.13)$$

The  $\alpha(i)$  value can be seen as the probability of the  $i^{th}$  input synapse to being active during the calcium spike period. The weights of the respective synapse were afterwards strengthened whenever the  $\alpha(i)$  value exceeded the adaptation threshold  $\vartheta_{adapt}$ . Otherwise the weight was weakened:

$$\text{If } \alpha(i) > \vartheta_{adapt} : \quad (5.14)$$

$$w_i = w_i \cdot \beta, \beta > 1.0$$

$$\text{If } \alpha(i) \leq \vartheta_{adapt} : \quad (5.15)$$

$$w_i = w_i \cdot \gamma, \gamma < 1.0$$

Depending on the weight adaptation factors  $\beta$  and  $\gamma$  the algorithm can be adjusted to converge very fast. However in some simulations where there

## 5 Implementation

is a lot of noise input, which may could also trigger output bursts, small adaptation factors might be feasible.

In contrast to the learning principle by [Körding and König, 2000] the weight updates are not based on the pre-synaptic firing rate. In this simulation only the influence of the synaptic input stream in comparison with all other input streams is determining whether the weight is strengthened or weakened. This update rule allows the pyramidal neuron model to specialize on specific synaptic input streams in an environment with small firing rates.

In the following example the first apical and the first basal input stream were active at the same time, triggering an output burst in the pyramidal neuron. As the rate of the apical input stream is slightly higher during the bursting period, the weight of the first apical input stream is more increased than the first basal input stream. All other inputs weights were weakened as they did not contribute to the bursts.

Figure 5.13 shows the initial behaviour of the pyramidal neuron. It can be observed that the first and the third apical input stream are active at the same rate, but only the first apical input stream (red) shows coincident activation with one of the basal input streams (blue), therefore triggering a single output burst.

Figures 5.14 visualizes the behaviour of the neuron after the weight adaptation. It is observable that the bursting mechanism was feasible for the neuron to specialize on the first apical input stream and ignoring all other activation. Due to this adaptation also minor coincidence between the first apical and first basal input stream now trigger a bursting behaviour.

## 5 Implementation

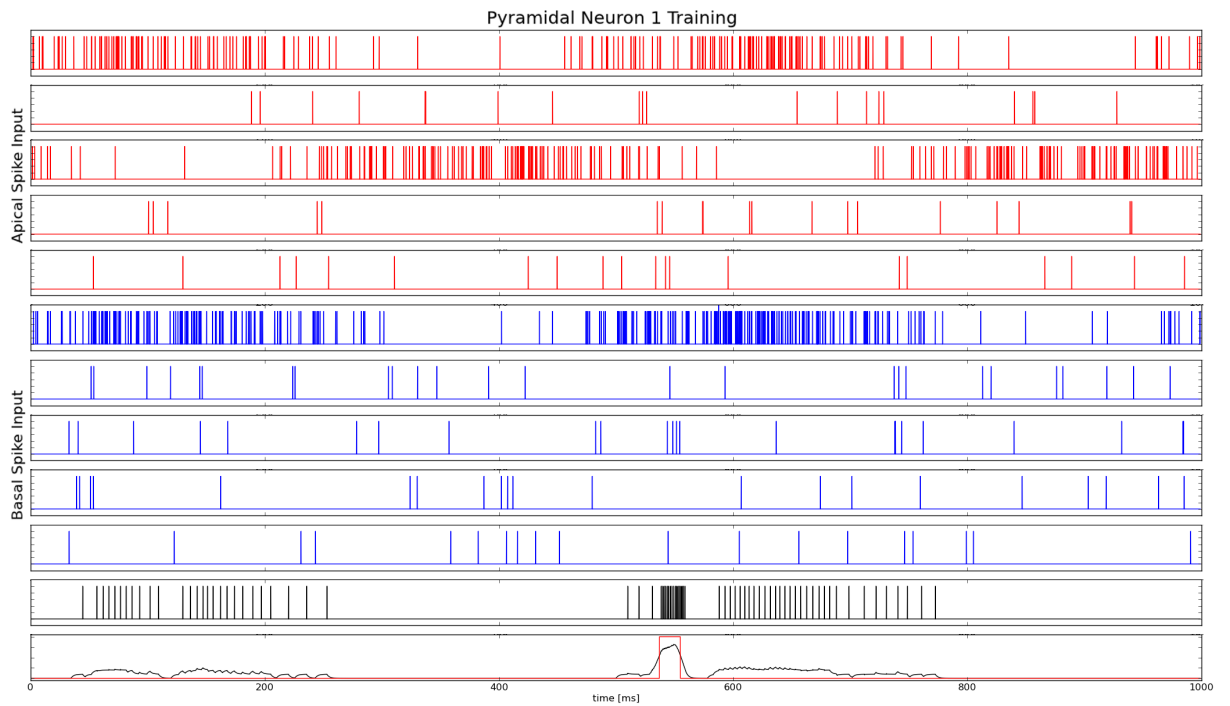


Figure 5.13: Input-Output behaviour of the pyramidal neuron for synchronous and asynchronous apical input. The figure shows the five input streams applied to the apical synapses (red) and the basal synapses (blue). The black spiking plot shows the output behaviour of the pyramid. The last plot finally shows the extracted output firing rate of the neuron, with bursts marked in red. The figure shows that the pyramidal neuron only shows activity whenever the apical (red) and basal (blue) input stream are active at the same time. If the activation is high enough a burst is triggered, which is used for learning. During the bursting period the synaptic weights of active inputs are strengthened, while inactive input weights are weakened. This leads to the output behaviour observable in figure 5.14

## 5 Implementation

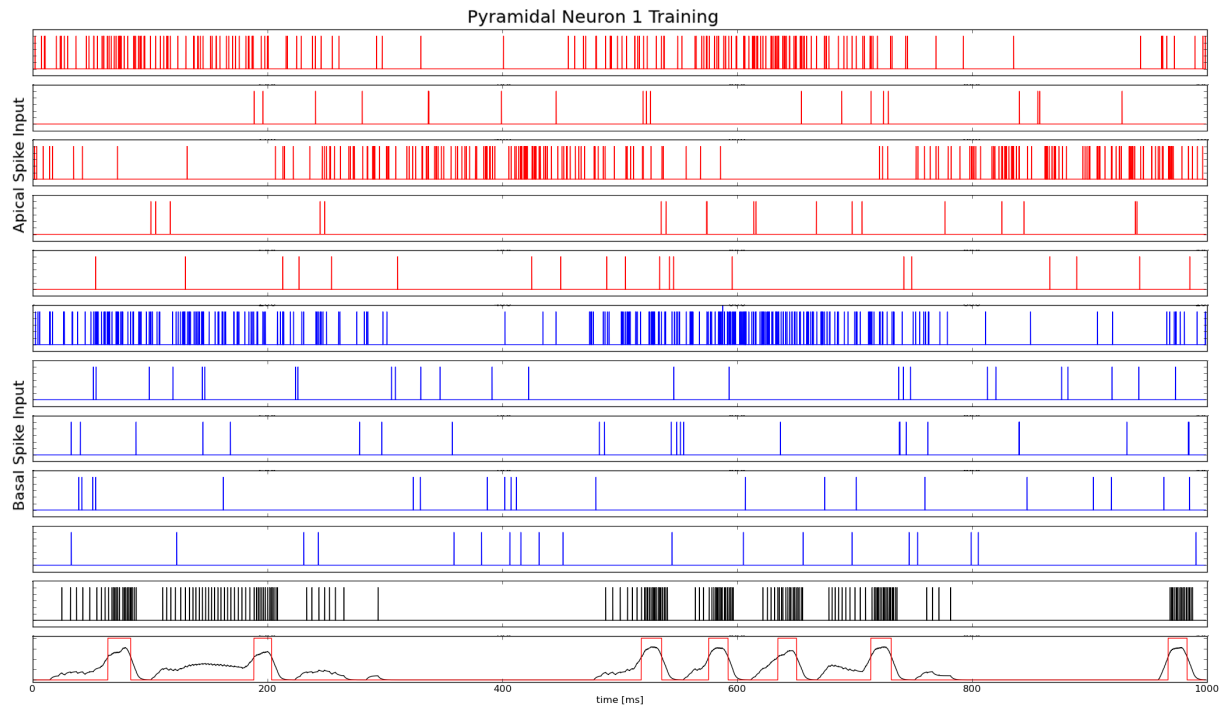


Figure 5.14: Input-Output behaviour of the pyramidal neuron for synchronous and asynchronous apical input after weight adaptation. The figure shows the final behaviour of the pyramidal neuron to the same input streams as in figure 5.13. During the bursts the synaptic weights of the active input streams (first apical input stream (red) and first basal input stream, blue) were strengthened, while the influence of the other inputs was weakened. This lead to a specialization of the pyramidal neuron on the first apical and first basal input stream, triggering more bursts whenever both are active.

The initial result of the second simulation can be seen in figure 5.15. It shows that the first and third basal input stream (blue) are active at a high rate. As all basal synaptic inputs are added and integrated in the basal compartment of the neuron, this leads to a constant activation and therefore a constant output spiking behaviour. Nevertheless an output burst is only triggered if the neuron also receives apical input (red).

Due to the weight adaptation during the bursts the neuron successfully specialized on the basal input synapses which were active during the bursts.

## 5 Implementation

The final behaviour of the model with adapted synaptic weights can be observed in figure 5.16.

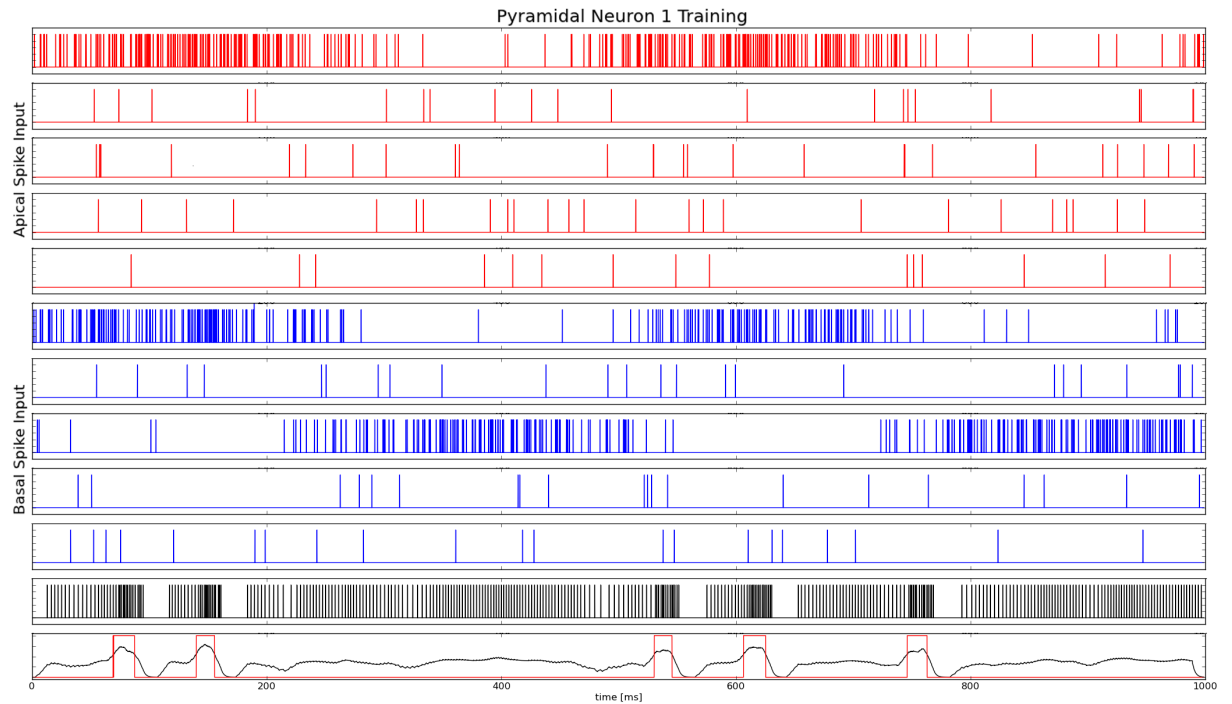


Figure 5.15: Input-Output behaviour of the pyramidal neuron for synchronous and asynchronous basal input. The figure shows the five input streams applied to the apical synapses (red) and the basal synapses (blue). The black spiking plot shows the output behaviour of the pyramid. The last plot finally shows the extracted output firing rate of the neuron, with bursts marked in red. The figure shows that the pyramidal neuron only shows activity whenever the apical (red) and basal (blue) input stream are active at the same time. If the activation is high enough a burst is triggered, which is used for learning. During the bursting period the synaptic weights of active inputs are strengthened, while inactive input weights are weakened. This leads to the output behaviour observable in figure 5.16

## 5 Implementation

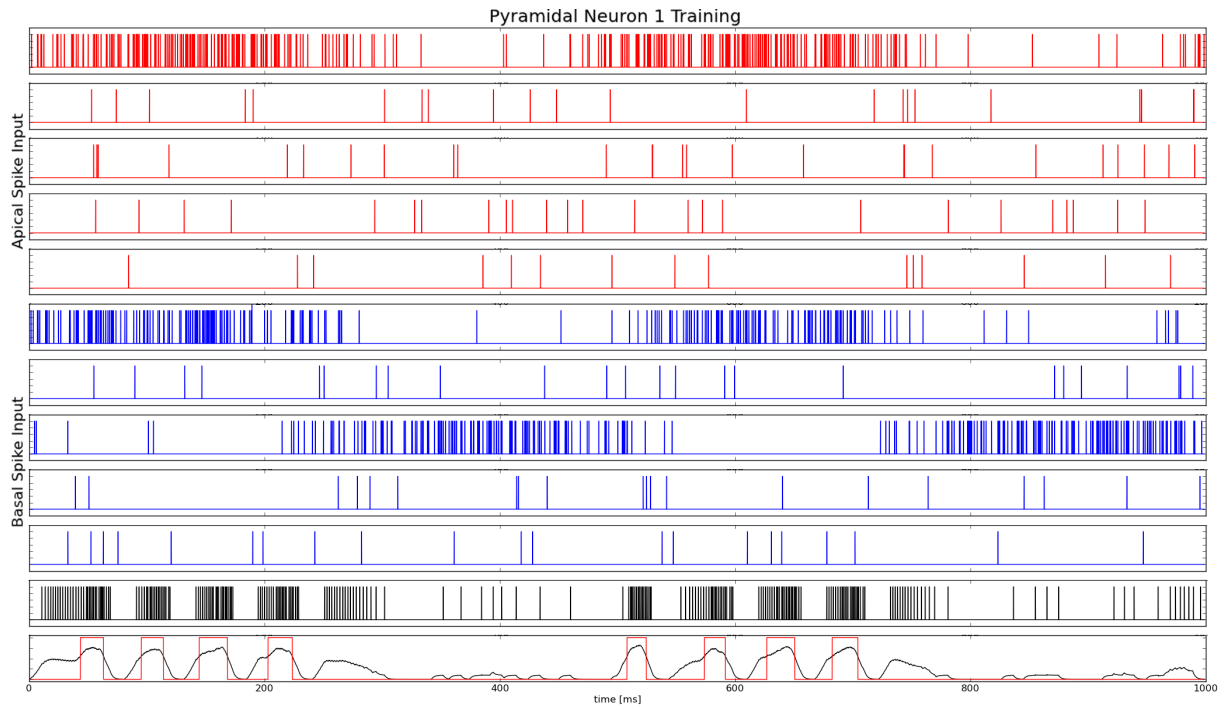


Figure 5.16: Input-Output behaviour of the pyramidal neuron for synchronous and asynchronous basal input after weight adaptation. The figure shows the final behaviour of the pyramidal neuron to the same input streams as in figure 5.15. During the bursts the synaptic weights of the active input streams (first apical input stream (red) and first basal input stream, blue) were strengthened, while the influence of the other inputs was weakened. This lead to a specialization of the pyramidal neuron on the first apical and first basal input stream, triggering more bursts whenever both are active. In comparison to the pre-learning situation, where the neuron showed an almost constant spiking behaviour, it now only shows activity according to its input streams it specialized on.

# 6 Conclusion

## 6.1 Results

The simulation results obtained in this thesis have shown to comply with experimental results obtained by [Richard Naud and Gerstner, 2013] and [Larkum, 2013]. It was further shown that by reformulating the model into a HMM representation, some parameters of the model can be obtained automatically.

The practical neuron model described here currently uses the intrinsic calcium spike mechanism to influence the spiking behaviour, triggering bursts whenever a feasible count of correlated input spikes arrive both at the basal and apical dendritic compartments. Theoretical findings suggest that the calcium spike is also a main factor in determining long term plasticity and learning in dendrites. Some papers (for example, [Körding and König, 2000], see description in chapter 2) have already focused on the influence of  $Ca^{2+}$  spikes on learning, while neglecting the effects on the output function of neurons.

The last simulation carried out (section 5.4.4) combined both effects of calcium spikes, using the extended spiking behaviour of the pyramidal neuron to trigger learning. In this case the output bursts, which occur during calcium spikes, were used to change the synaptic weights of input synapses which were active during the bursting period. It could therefore be shown that the pyramidal neuron is not only able to combine two independent information streams arriving at its apical and basal dendrites, which reflects in its output spiking behaviour. The neuron model is also able to adapt its synaptic weights, specializing on the input streams which trigger the calcium spiking mechanism.

### 6.2 Outlook

With the inclusion of calcium spikes and their resulting bursting behaviour, bursting events can be added to single spike events and their respective timing as the main information in spiking neuron networks.

In the last simulation the bursting behaviour was already used to trigger synaptic plasticity in a single pyramidal neuron. However only the neuron triggering the bursts adapted its synaptic weights. In future simulations the bursting behaviour and especially the reaction of other pyramidal neurons or interneurons in the cortex on bursts could be considered.

The question whether postsynaptic neurons are able to detect bursts and forward the information has already been addressed [[Larkum et al., 2004](#)]. The paper states an interesting fact, namely that the coincidence time window between feedforward input arriving at the proximal dendrites and feedback input arriving distally is about 30ms, which is about the same duration of a triggered burst. This leads to the question of whether this level of precision holds a special significance in the neocortex.

The importance of bursts was also acknowledged by experiments performed during slow-wave sleep. During this phase the former experience patterns were repeated automatically at a higher frequency, triggering active bursts in the neocortex. Including the ability of postsynaptic neurons to detect and react to this bursting behaviour could lead to the assumption that bursts are a main determining factor for memory [[Paulsen and Sejnowski, 2000](#)].

# Appendix

## References

- [Allen, ] Allen, J. Efficient methods for training hmms. [www.cs.rochester.edu/u/james/CSC248/Lec11.pdf](http://www.cs.rochester.edu/u/james/CSC248/Lec11.pdf).
- [Antic et al., 2010] Antic, S. D., Zhou, W.-L., Moore, A. R., Short, S. M., and Ikonomu, K. D. (2010). The decade of the dendritic nmda spike. *Journal of neuroscience research*, 88(14):2991–3001.
- [Behabadi and Mel, 2014] Behabadi, B. F. and Mel, B. W. (2014). Mechanisms underlying subunit independence in pyramidal neuron dendrites. *Proceedings of the National Academy of Sciences*, 111(1):498–503.
- [Bengio and Frasconi, 1995] Bengio, Y. and Frasconi, P. (1995). An input output hmm architecture. *Advances in neural information processing systems*, pages 427–434.
- [Benuskova, 2003] Benuskova (2003). Spiking neuron model and spike-timing dependent plasticity.
- [Berman and Maler, 1999] Berman, N. J. and Maler, L. (1999). Neural architecture of the electrosensory lateral line lobe: adaptations for coincidence detection, a sensory searchlight and frequency-dependent adaptive filtering. *Journal of Experimental Biology*, 202(10):1243–1253.
- [Bi and Poo, 1998] Bi, G.-q. and Poo, M.-m. (1998). Synaptic modifications in cultured hippocampal neurons: dependence on spike timing, synaptic strength, and postsynaptic cell type. *The Journal of neuroscience*, 18(24):10464–10472.
- [Brette et al., 2007] Brette, R., Rudolph, M., Carnevale, T., Hines, M., Berman, D., Bower, J. M., Diesmann, M., Morrison, A., Goodman, P. H., and Harris Jr, F. C. (2007). Simulation of networks of spiking neurons: a review of tools and strategies. *Journal of computational neuroscience*, 23(3):349–398.

## References

- [Burkitt, 2006] Burkitt, A. N. (2006). A review of the integrate-and-fire neuron model: I. homogeneous synaptic input. *Biological cybernetics*, 95(1):1–19.
- [Buzsaki, 2004] Buzsaki, G. (2004). Large-scale recording of neuronal ensembles. *Nature neuroscience*, 7(5):446–451.
- [Crick and Koch, 1998] Crick, F. and Koch, C. (1998). Consciousness and neuroscience. *Cerebral cortex*, 8(2):97–107.
- [Destexhe and Pare, 1999] Destexhe, A. and Pare, D. (1999). Impact of network activity on the integrative properties of neocortical pyramidal neurons in vivo. *Journal of Neurophysiology*, 81(4):1531–1547.
- [Diesmann and Gewaltig, 2001] Diesmann, M. and Gewaltig, M.-O. (2001). Nest: An environment for neural systems simulations. *Forschung und wissenschaftliches Rechnen, Beiträge zum Heinz-Billing-Preis*, 58:43–70.
- [Elston, 2003] Elston, G. N. (2003). Cortex, cognition and the cell: new insights into the pyramidal neuron and prefrontal function. *Cerebral Cortex*, 13(11):1124–1138.
- [Fourcaud-Trocme et al., 2003] Fourcaud-Trocme, N., Hansel, D., Van Vreeswijk, C., and Brunel, N. (2003). How spike generation mechanisms determine the neuronal response to fluctuating inputs. *The Journal of neuroscience*, 23(37):11628–11640.
- [Gerstner and Kistler, 2002] Gerstner, W. and Kistler, W. M. (2002). *Spiking neuron models: Single neurons, populations, plasticity*. Cambridge university press.
- [Hattox and Nelson, 2007] Hattox, A. M. and Nelson, S. B. (2007). Layer v neurons in mouse cortex projecting to different targets have distinct physiological properties. *Journal of neurophysiology*, 98(6):3330–3340.
- [Häusser and Mel, 2003] Häusser, M. and Mel, B. (2003). Dendrites: bug or feature? *Current opinion in neurobiology*, 13(3):372–383.
- [Häusser et al., 2000] Häusser, M., Spruston, N., and Stuart, G. J. (2000). Diversity and dynamics of dendritic signaling. *Science*, 290(5492):739–744.

## References

- [Helmchen et al., 1999] Helmchen, F., Svoboda, K., Denk, W., and Tank, D. W. (1999). In vivo dendritic calcium dynamics in deep-layer cortical pyramidal neurons. *Nature neuroscience*, 2(11):989–996.
- [Hirsch et al., 1995] Hirsch, J. A., Alonso, J.-M., and Reid, R. C. (1995). Visually evoked calcium action potentials in cat striate cortex. pages –.
- [Hirsch et al., 1974] Hirsch, M. W., Devaney, R. L., and Smale, S. (1974). *Differential equations, dynamical systems, and linear algebra*, volume 60. Access Online via Elsevier.
- [Ilan et al., 2011] Ilan, L. B., Gidon, A., and Segev, I. (2011). Interregional synaptic competition in neurons with multiple stdp-inducing signals. *Journal of neurophysiology*, 105(3):989–998.
- [Initiative, 2014] Initiative, N. (2014). Nest simulator. [http://www.nest-initiative.org/Software>About\\_NEST](http://www.nest-initiative.org/Software>About_NEST).
- [Jadi et al., 2012] Jadi, M., Polsky, A., Schiller, J., and Mel, B. W. (2012). Location-dependent effects of inhibition on local spiking in pyramidal neuron dendrites. *PLoS computational biology*, 8(6):e1002550.
- [Jolivet et al., 2006] Jolivet, R., Rauch, A., Lüscher, H.-R., and Gerstner, W. (2006). Predicting spike timing of neocortical pyramidal neurons by simple threshold models. *Journal of computational neuroscience*, 21(1):35–49.
- [Kim et al., 1995] Kim, H., Beierlein, M., and Connors, B. W. (1995). Inhibitory control of excitable dendrites in neocortex. *Journal of neurophysiology*, 74(4):1810–1814.
- [Kistler et al., 1997] Kistler, W. M., Gerstner, W., and van Hemmen, J. L. (1997). Reduction of the hodgkin-huxley equations to a single-variable threshold model. *Neural Computation*, 9(5):1015–1045.
- [Koch and Segev, 2000] Koch, C. and Segev, I. (2000). The role of single neurons in information processing. *nature neuroscience*, 3:1171–1177.
- [Körding and König, 2000] Körding, K. P. and König, P. (2000). Learning with two sites of synaptic integration. *Network: Computation in neural systems*, 11(1):25–39.

## References

- [Körding and König, 2001] Körding, K. P. and König, P. (2001). Supervised and unsupervised learning with two sites of synaptic integration. *11*(3):207–215.
- [Larkum, 2013] Larkum, M. (2013). A cellular mechanism for cortical associations: an organizing principle for the cerebral cortex. *Trends in Neurosciences*, *36*(3):141–151.
- [Larkum et al., 2009] Larkum, M. E., Nevian, T., Sandler, M., Polsky, A., and Schiller, J. (2009). Synaptic integration in tuft dendrites of layer 5 pyramidal neurons: a new unifying principle. *Science*, *325*(5941):756–760.
- [Larkum et al., 2004] Larkum, M. E., Senn, W., and Löscher, H.-R. (2004). Top-down dendritic input increases the gain of layer 5 pyramidal neurons. *Cerebral Cortex*, *14*(10):1059–1070.
- [Larkum and Zhu, 2002] Larkum, M. E. and Zhu, J. J. (2002). Signaling of layer 1 and whisker-evoked ca<sup>2+</sup> and na<sup>+</sup> action potentials in distal and terminal dendrites of rat neocortical pyramidal neurons in vitro and in vivo. *The Journal of neuroscience*, *22*(16):6991–7005.
- [Larkum et al., 1999] Larkum, M. E., Zhu, J. J., and Sakmann, B. (1999). A new cellular mechanism for coupling inputs arriving at different cortical layers. *Nature*, *398*(6725):338–341.
- [Larkum et al., 2001] Larkum, M. E., Zhu, J. J., and Sakmann, B. (2001). Dendritic mechanisms underlying the coupling of the dendritic with the axonal action potential initiation zone of adult rat layer 5 pyramidal neurons. *The Journal of physiology*, *533*(2):447–466.
- [Major et al., 2013] Major, G., Larkum, M. E., and Schiller, J. (2013). Active properties of neocortical pyramidal neuron dendrites. *Annu. Rev. Neurosci.*, *36*(1):1–24.
- [Manns et al., 2004] Manns, I. D., Sakmann, B., and Brecht, M. (2004). Sub- and suprathreshold receptive field properties of pyramidal neurones in layers 5a and 5b of rat somatosensory barrel cortex. *The Journal of physiology*, *556*(2):601–622.

## References

- [Markram et al., 1998] Markram, H., Wang, Y., and Tsodyks, M. (1998). Differential signaling via the same axon of neocortical pyramidal neurons. *Proceedings of the National Academy of Sciences*, 95(9):5323–5328.
- [Merker, 2007] Merker, B. (2007). Consciousness without a cerebral cortex: A challenge for neuroscience and medicine. *Behavioral and Brain Sciences*, 30(01):63–81.
- [Miles et al., 1996] Miles, R., Toth, K., Gulyas, A. I., Hajos, N., and Freund, T. F. (1996). Differences between somatic and dendritic inhibition in the hippocampus. *Neuron*, 16(4):815–823.
- [Murayama and Larkum, 2009] Murayama, M. and Larkum, M. E. (2009). Enhanced dendritic activity in awake rats. *Proceedings of the National Academy of Sciences*, 106(48):20482–20486.
- [Paninski et al., 2003] Paninski, L., Lau, B., and Reyes, A. (2003). Noise-driven adaptation: in vitro and mathematical analysis. *Neurocomputing*, 52:877–883.
- [Paninski et al., 2004] Paninski, L., Pillow, J. W., and Simoncelli, E. P. (2004). Maximum likelihood estimation of a stochastic integrate-and-fire neural encoding model. *Neural computation*, 16(12):2533–2561.
- [Pare et al., 1998] Pare, D., Lang, E., and Destexhe, A. (1998). Inhibitory control of somatodendritic interactions underlying action potentials in neocortical pyramidal neurons *in vivo*: An intracellular and computational study. *Neuroscience*, 84(2):377–402.
- [Paulsen and Sejnowski, 2000] Paulsen, O. and Sejnowski, T. J. (2000). Natural patterns of activity and long-term synaptic plasticity. *Current Opinion in Neurobiology*, 10(2):172–180.
- [Perez-Garci et al., 2013] Perez-Garci, E., Larkum, M. E., and Nevian, T. (2013). Inhibition of dendritic  $Ca^{2+}$  spikes by gabab receptors in cortical pyramidal neurons is mediated by a direct  $g_i/o$ -subunit interaction with  $cav1$  channels. *The Journal of physiology*, 591(7):1599–1612.
- [Pike et al., 1999] Pike, F. G., Meredith, R. M., Olding, A. W., and Paulsen, O. (1999). Postsynaptic bursting is essential for Hebbian induction of associative long-term potentiation

## References

- at excitatory synapses in rat hippocampus. *The Journal of Physiology*, 518(2):571–576.
- [Poirazi et al., 2003] Poirazi, P., Brannon, T., and Mel, B. W. (2003). Pyramidal neuron as two-layer neural network. *Neuron*, 37(6):989–999.
- [Poirazi and Mel, 2001] Poirazi, P. and Mel, B. W. (2001). Impact of active dendrites and structural plasticity on the memory capacity of neural tissue. *Neuron*, 29(3):779–796.
- [Polsky et al., 2004] Polsky, A., Mel, B. W., and Schiller, J. (2004). Computational subunits in thin dendrites of pyramidal cells. *Nature neuroscience*, 7(6):621–627.
- [Rapp et al., 1996] Rapp, M., Yarom, Y., and Segev, I. (1996). Modeling back propagating action potential in weakly excitable dendrites of neocortical pyramidal cells. *Proceedings of the National Academy of Sciences*, 93(21):11985–11990.
- [Rhodes, 2006] Rhodes, P. (2006). The properties and implications of nmda spikes in neocortical pyramidal cells. *The Journal of neuroscience*, 26(25):6704–6715.
- [Richard Naud and Gerstner, 2013] Richard Naud, B. B. and Gerstner, W. (2013). Spike-timing prediction with active dendrites.
- [Rotter and Diesmann, 1999] Rotter, S. and Diesmann, M. (1999). Exact digital simulation of time-invariant linear systems with applications to neuronal modeling. *Biological Cybernetics*, 81(5-6):381–402.
- [Ryder and Favorov, 2001] Ryder, D. and Favorov, O. V. (2001). The new associationism: a neural explanation for the predictive powers of cerebral cortex. *Brain and Mind*, 2(2):161–194.
- [Schaefer et al., 2003] Schaefer, A. T., Larkum, M. E., Sakmann, B., and Roth, A. (2003). Coincidence detection in pyramidal neurons is tuned by their dendritic branching pattern. *Journal of neurophysiology*, 89(6):3143–3154.
- [Schiller et al., 2000] Schiller, J., Major, G., Koester, H. J., and Schiller, Y. (2000). Nmda spikes in basal dendrites of cortical pyramidal neurons. *Nature*, 404(6775):285–289.

## References

- [Schiller et al., 1997] Schiller, J., Schiller, Y., Stuart, G., and Sakmann, B. (1997). Calcium action potentials restricted to distal apical dendrites of rat neocortical pyramidal neurons. *The Journal of physiology*, 505(3):605–616.
- [Scholarpedia, 2013a] Scholarpedia (2013a). Models of synaptic plasticity. [http://www.scholarpedia.org/article/Models\\_of\\_synaptic\\_plasticity](http://www.scholarpedia.org/article/Models_of_synaptic_plasticity).
- [Scholarpedia, 2013b] Scholarpedia (2013b). Pyramidal neuron. [http://www.scholarpedia.org/article/Pyramidal\\_neuron](http://www.scholarpedia.org/article/Pyramidal_neuron).
- [Scholarpedia, 2014] Scholarpedia (2014). Spike response model. [http://www.scholarpedia.org/article/Spike\\_response\\_model](http://www.scholarpedia.org/article/Spike_response_model).
- [Siegel et al., 2000] Siegel, M., Körding, K. P., and König, P. (2000). Integrating top-down and bottom-up sensory processing by somato-dendritic interactions. *Journal of computational neuroscience*, 8(2):161–173.
- [Sjöström and Nelson, 2002] Sjöström, P. J. and Nelson, S. B. (2002). Spike timing, calcium signals and synaptic plasticity. *Current opinion in neurobiology*, 12(3):305–314.
- [Sjöström et al., 2008] Sjöström, P. J., Rancz, E. A., Roth, A., and Häusser, M. (2008). Dendritic excitability and synaptic plasticity. *Physiological Reviews*, 88(2):769–840.
- [Sourd et al., 1999] Sourd, V. and Debanne, D. (1999). The role of dendritic filtering in associative long-term synaptic plasticity. *Learning & Memory*, 6(5):422–447.
- [Spratling, 2002] Spratling, M. (2002). Cortical region interactions and the functional role of apical dendrites. *Behavioral and Cognitive Neuroscience Reviews*, 1(3):219–228.
- [Spruston, 2008] Spruston, N. (2008). Pyramidal neurons: dendritic structure and synaptic integration. *Nature Reviews Neuroscience*, 9(3):206–221.
- [Squire, 2004] Squire, L. R. (2004). Memory systems of the brain: a brief history and current perspective. *Neurobiology of learning and memory*, 82(3):171–177.

## References

- [Stuart et al., 1997] Stuart, G., Spruston, N., Sakmann, B., and Häusser, M. (1997). Action potential initiation and backpropagation in neurons of the mammalian CNS. *Trends in neurosciences*, 20(3):125–131.
- [Stuart and Sakmann, 1994] Stuart, G. J. and Sakmann, B. (1994). Active propagation of somatic action potentials into neocortical pyramidal cell dendrites. *Nature*, 367(6458):69–72.
- [Tsubokawa and Ross, 1996] Tsubokawa, H. and Ross, W. N. (1996). Ipsps modulate spike backpropagation and associated  $[Ca^{2+}]_i$  changes in the dendrites of hippocampal CA1 pyramidal neurons. *Journal of Neurophysiology*, 76(5):2896–2906.
- [Wang et al., 2006] Wang, Y., Markram, H., Goodman, P. H., Berger, T. K., Ma, J., and Goldman-Rakic, P. S. (2006). Heterogeneity in the pyramidal network of the medial prefrontal cortex. *Nature neuroscience*, 9(4):534–542.
- [Williams and Stuart, 2002] Williams, S. R. and Stuart, G. J. (2002). Dependence of EPSP efficacy on synapse location in neocortical pyramidal neurons. *Science*, 295(5561):1907–1910.
- [Xu et al., 2012] Xu, N.-l., Harnett, M. T., Williams, S. R., Huber, D., O'Connor, D. H., Svoboda, K., and Magee, J. C. (2012). Nonlinear dendritic integration of sensory and motor input during an active sensing task. *Nature*, 492(7428):247–251.